

1 **CFNTT: Scalable Radix-2/4 NTT Multiplication**
2 **Architecture with an Efficient Conflict-free**
3 **Memory Mapping Scheme**

4 Anonymous Submission

5 **Abstract.** Number theoretic transform (NTT) can be utilized to speed up polynomial
6 multiplication, which is the critical computation bottleneck in a lot of cryptographic
7 algorithms like lattice-based post-quantum cryptography (PQC) and homomorphic
8 encryption (HE). The NTT hardware architecture needs to support diverse security
9 parameters and meet resource constraints on different computing platforms. Thus
10 flexibility and Area-Time Product (ATP) become two crucial metrics in NTT hardware
11 design. The flexibility of NTT in terms of different vector sizes and moduli can be
12 obtained directly. Whereas the varying strides in memory access of in-place NTT
13 render the configuration for different radix and number of parallel butterfly units
14 a tough problem. This paper proposes an efficient conflict-free memory mapping
15 scheme which supports the configuration for both multiple parallel butterfly units
16 and arbitrary radix of NTT. Compared to other approaches, this scheme owns a
17 wider application and facilitates the parallelization of non-radix-2 NTT hardware
18 design. Based on this scheme, we propose a scalable radix-2 and radix-4 NTT
19 multiplication architecture by algorithm-hardware co-design. A versatile schedule
20 method is leveraged to reduce the number of modular additions/subtractions and
21 modular multiplications of radix-4 butterfly unit by 20% and 33%, respectively. To
22 avoid the bit-reversed cost and save memory footprint in arbitrary radix NTT/INTT,
23 we put forward a general method by rearranging the loop structure and reusing the
24 twiddle factors. The architecture-level optimization is achieved by excavating the
25 symmetric operators in radix-4 butterfly unit, which saves almost 50% hardware
26 resources compared to a straightforward implementation. Through experimental
27 results and theoretical analysis, we point out that the radix-4 NTT with the same
28 number of parallel butterfly units outperforms the radix-2 NTT in terms of area-time
29 performance in the interleaved memory system. This advantage is enlarged when
30 increasing the number of parallel butterfly units. For example, when processing 1024
31 14-bit points NTT with 8 parallel butterfly units, the ATP of radix-4 NTT FPGA
32 core achieves improvement by approximately 51.6%.

33 **Keywords:** number theoretic transform, polynomial multiplication, algorithm-hardware
34 co-design, radix-4, conflict-free memory mapping scheme

35 **1 Introduction**

36 In recent years, both industrial and academic community have sparked a boom in the
37 research of post-quantum cryptography and homomorphism encryption. Since the Shor
38 algorithm renders the traditional cryptosystems, like Rivest Shamir Adleman (RSA) and
39 Elliptic Curve Cryptography (ECC), to be cracked by quantum computer within polynomial
40 time [Sho94], the National Institute of Standards and Technology (NIST) has initiated a
41 contest to solicit anti-quantum cryptographic algorithms around the world. In July 2020, 7
42 finalists and the 8 alternate candidates are announced in the third round and lattice-based
43 schemes account for 5/7 of them. Lattice-based cryptography provides both solid security
44 and hardware friendly way to build anti-quantum cryptosystems [MAA⁺20]. It also offers

other advanced applications, such as fully homomorphic encryption [Gen09] and zero knowledge proof [LNS20]. Homomorphic encryption algorithm enables the computation process of data in the form of ciphertext, further ensuring the privacy of server-side data. The polynomial multiplication is the well-known computational bottleneck in lattice-based schemes, while leveraging number theoretic transform can reduce its complexity from $\mathcal{O}(N^2)$ to $\mathcal{O}(N \log N)$ [Nic71]. As a result, works focused on the design of NTT hardware accelerator have been intensively carried out.

Although the NTT algorithm applied in lattice-based PQC and HE is slightly different, the overall hardware architecture has a lot of similarity. It is interesting to propose a scalable NTT multiplication architecture as a building block for these schemes [CHK⁺21] [MKO⁺20a]. Besides, some resource constrained scenarios focus on compact and energy-efficient design like IoT, while others pursue high throughput and better performance like 5G [XHY⁺20]. To meet these diverse requirements, the flexibility and Area-Time Product become two crucial metrics in NTT hardware design.

Related work. Plenty of works have developed optimization techniques for radix-2 NTT hardware architecture. But the design of radix-4 NTT hardware core is still rare. With regard to the algorithm level optimization, [POG15] and [ZCY⁺20] demonstrate the iterative radix-2 NTT algorithm free from the pre-processing and post-processing. It reduces the computation complexity by merging the $2N$ -th primitive roots of unity and scale factor into every stage. [XL21] and [POG15] avoid the bit-reversed cost by changing the loop structure of decimation in time (DIT) and decimation in frequency (DIF) radix-2 NTT. This method is also adopted by the reference software implementation of Kyber published by NIST. [ACC⁺21] and [CHK⁺21] introduce various NTT extension algorithms by applying versatile FFT tricks, enabling the software implementation of polynomial multiplication on NTT unfriendly rings. In terms of architecture level design, unlike the popular pipelined FFT architecture, such as single delay feedback (SDF) and multiple delay commutator (MDC) [TCH19] [HT96], current NTT core mainly adopts memory-based architecture allowing for trade-off between area and performance. [CMV⁺15] proposes a high-speed pipelined polynomial multiplication architecture based on constant geometry radix-2 NTT. This paper points out the temporal conflicts in pipelined architecture. [FL19] presents a HE integer multiplier utilizing the negative wrapped convolution and Ping-pong radix-2 FFT algorithm. Compared to in-place NTT architecture, the aforementioned two types have simpler memory access pattern at the price of double memory overheads. Actually, [GGMG13] and [SYJ84] indicate that radix-4 FFT architecture has advantages in high-throughput-demanding applications.

Conflict-free memory mapping scheme is a key component for parallel NTT hardware architecture. However, to our best knowledge, efficient and general memory mapping scheme for arbitrary radix NTT with parallel butterfly units is still in lack. [Joh92] presents a conflict-free address mapping method for arbitrary radix FFT. [LSW01] and [WHEW14] design a dedicated radix-2 FFT and radix-16 NTT architecture based on this method, respectively. But it is identified in [XMX17] and [ZCY⁺20] that this scheme cannot be applied into the case when placing multiple parallel butterfly units into every stage. [ZCY⁺20] handles this problem by changing the last loop of NTT algorithm, but it is only suitable for radix-2 NTT. [XMX17] [TJS03] presents a memory mapping approach in terms of radix- 2^k constant geometry FFT configured with several parallel butterfly units. The vector radix-2 NTT core configured with 32 parallel butterfly units is proposed in [XHY⁺20]. The memory access pattern is implemented by six types of permutation networks, which has complex control mode and consumes more hardware resources. [RV08] puts forward an address mapping scheme supporting arbitrary radix in-place FFT and parallel butterfly units. But this scheme requires a lot of banks positioning at every stage as read-write buffer. Memory mapping approach proposed in [RMD⁺15] will vary with

97 stages, increasing the complexity of pipelined design. A constant geometry radix-2 NTT
 98 architecture with only two parallel butterfly units is demonstrated in [BUC19]. [FLX20]
 99 also proposes a parallel Stockham NTT hardware design. [XWXY17] derives an address
 100 mapping approach for parallel arbitrary radix MDC-memory-based FFT architecture.
 101 However, the aforementioned three cases consume double memory overheads. [MKÖ⁺20b]
 102 and [RVM⁺14] utilize a single RAM to construct the parallel radix-2 NTT address mapping
 103 scheme without consideration for other radix.

104

105 **Contribution.** In general, our contributions are summarized as follows:

- 106 1. We provide a detailed derivation for bit-reversed-free radix-4 NTT/INTT algorithm
 107 with low complexity over polynomial rings. The proposed algorithm eliminates the
 108 pre-processing and post-processing by merging $2N$ -th primitive roots of unity and
 109 scale factors into every stage of radix-4 NTT/INTT, which consumes minimal number
 110 of modular multiplications $N \log_4 N$. To avoid the bit-reversed cost and reduce the
 111 memory footprint in arbitrary radix NTT/INTT, we put forward a general method
 112 by rearranging the loop structure and reusing the twiddle factors.
- 113 2. A scalable radix-2 and radix-4 NTT multiplication architecture is proposed in this
 114 paper. We adopt a versatile schedule method to reduce the number of modular
 115 additions/subtractions and multiplications in radix-4 butterfly unit by 20% and
 116 30%, respectively. By excavating and reusing the symmetric operators in radix-4
 117 butterfly unit, we saves almost 50% area overheads compared to a straightforward
 118 implementation. Through experimental results and theoretical analysis, we point
 119 out that the radix-4 NTT has an advantage over radix-2 NTT in terms of area-time
 120 performance in the interleaved memory system, which is enlarged when increasing
 121 the number of parallel butterfly units. The ATP of radix-4 NTT FPGA core
 122 with 8 parallel butterfly units achieves improvement by approximately 51.6% when
 123 processing 1024 14-bit points NTT.
- 124 3. The efficient memory access of in-place NTT is guaranteed by the proposed conflict-
 125 free mapping scheme, which supports the configuration for multiple parallel butterfly
 126 units and arbitrary radix. This scheme avoids introducing queues and pipeline stalls,
 127 thus enabling the 100% utilization of pipelined NTT architecture. It also paves the
 128 way for other non-radix-2 NTT hardware design. In contrast to other approaches,
 129 this scheme has a wider application and can be implemented by standard logic gates
 130 like bit-wise XORs and Shifts.

131 2 Preliminaries

132 2.1 NTT-based Multiplication Algorithm

133 The traditional Fast Fourier Transform (FFT) applied in digital signal process is defined
 134 on the complex field \mathbb{C} , which reduces the computation complexity of Discrete Fourier
 135 Transform (DFT) from $\mathcal{O}(N^2)$ to $\mathcal{O}(N \log N)$. The Number Theoretical Transform (NTT)
 136 can be regarded as DFT defined on finite field \mathbb{Z}_q , so that the vector multiplication can
 137 be computed without loss accuracy. The Inverse Number Theoretical Transform (INTT)
 138 can be obtained by replacing the twiddle factor ω of NTT with its inverse element ω^{-1}
 139 followed by multiplying the scale factor N^{-1} . The concrete formula is described as belows:

140 [Nic71]:

$$\begin{aligned} A_i &= NTT(a_i) = \sum_{j=0}^{N-1} a_j \omega_N^{ij} \bmod q \quad i = 0, 1, \dots, N-1 \\ 141 \quad a_j &= INTT(A_j) = -\frac{1}{N} \sum_{i=0}^{N-1} A_i \omega_N^{-ij} \bmod q \quad j = 0, 1, \dots, N-1 \end{aligned} \quad (1)$$

142 **NTT multiplication on finite field.** In general, the prime modulus q needs to satisfy
 143 $q \equiv 1 \pmod{N}$, which ensures the existence of N -th primitive roots of unity ω . N is a
 144 power of 2. As a result, the multiplication of two N -term polynomials on finite field can
 145 be performed as equation 2, where the length of vector \mathbf{a} and \mathbf{b} is N , the zeropadding
 146 operation is to double the length of input vector by appending N zero at the end. Therefore,
 147 the length of vector \mathbf{c} becomes $2N$.

$$148 \quad \mathbf{c} = INTT(NTT(zeropadding(\mathbf{a})) \cdot NTT(zeropadding(\mathbf{b}))) \quad (2)$$

149 **NTT multiplication over the ring.** In lattice-based PQC algorithm, the polynomial
 150 multiplication over the ring $\mathbb{Z}_q[x]/\langle f(x) \rangle$ needs extra modular reduction with irreducible
 151 polynomial $f(x)$. But if $f(x) = x^N + 1$, we can use the well-known negative wrapped
 152 convolution (NWC) method to avoid doubling efforts and extra modular reduction. The
 153 NWC method can be expressed as equation 3, where ϕ is $2N$ -th roots of unity and $q \equiv 1$
 154 ($\pmod{2N}$) at this time.

$$\begin{aligned} 155 \quad \text{Pre-processing : } \bar{a}_i &= a_i \cdot \phi_{2N}^i \quad \bar{b}_i = b_i \cdot \phi_{2N}^i \\ \text{Multiplication : } \bar{c}_i &= INTT(NTT(\bar{a}_i) \cdot NTT(\bar{b}_i)) \\ \text{Post-processing : } c_i &= \bar{c}_i \cdot \phi_{2N}^{-i} \end{aligned} \quad (3)$$

156 The so-called pre-processing and post-processing can be eliminated by merging factors
 ϕ_{2N}^i (ϕ_{2N}^{-i}) into every stages of NTT [ZYC⁺20]. While the bit-reversed operation can be

Algorithm 1 Radix-2 Bit-reversed-free DIT NTT Algorithm

Input: \mathbf{a} denotes a vector of length N , q is modulus and ϕ_{2N} is $2N$ -th primitive roots of unity.

Output: $\mathbf{A} = DIT_NTT(\mathbf{a})$

```

1:  $r \leftarrow 1$ 
2: for  $p = \log_2 N - 1$  to 0 do
3:    $J \leftarrow 2^p$ 
4:    $\omega_m \leftarrow \phi_{2N}^{N/(2J)}$ 
5:   for  $k = 0$  to  $N/(2J) - 1$  do
6:      $\omega \leftarrow \omega_m^{\text{bit-reversed}(r)}$ 
7:      $r \leftarrow r + 1$ 
8:     for  $j = 0$  to  $J - 1$  do
9:        $u \leftarrow A_{2kJ+j}$ 
10:       $v \leftarrow A_{2kJ+j+J}$ 
11:       $A_{2kJ+j} \leftarrow (u + v \cdot \omega) \bmod q$ 
12:       $A_{2kJ+j+J} \leftarrow (u - v \cdot \omega) \bmod q$ 
13:     end for
14:   end for
15: end for
16: return  $\mathbf{A}$ 

```

157 further removed by rearranging the loop structure [XL21]. The complete bit-reversed-free
 158 radix-2 iterative NTT with low complexity is presented in algorithm 1, where the twiddle
 159 factors ω can be precomputed and stored in the ROM. [ACC⁺21] and [CHK⁺21] introduce
 160 a series of NTT extension algorithms, e.g., mixed-radix, Good's trick and multiple modulus
 161 NTT, which allows the NTT multiplication to be performed on NTT-unfriendly rings.
 162 However, these novel algorithms are only implemented on the software platform Cortex-M4
 163

164 and AVX2.

165 **Radix- 2^k NTT algorithm.** The appearance of radix- 2^2 is a milestone in FFT hardware
 166 design, which is extended to radix- 2^k later [GGMG13]. The radix-4 FFT is preferable to
 167 be applied in high-throughput-demanding applications [SYJ84]. In analogy with FFT, we
 168 can also obtain the radix- 2^k NTT algorithm. Actually, in [ABCG20] [BKS19] [GOPS13]
 169 [CHK⁺21], the radix- 2^k NTT algorithm is realized by merging multiple layers of radix-2
 170 NTT on the resource-constrained micro-controller platforms. This method is leveraged
 171 to reduce the cache loading and storing overheads. In this paper, we will provide the
 172 detailed derivation of bit-reversed-free radix-4 NTT/INTT algorithm with low computation
 173 complexity. Furthermore, we point out that its hardware advantage in terms of better
 174 area-timing trade-off is benefited from the symmetric operators and less number of banks.
 175 **Properties of twiddle factor.** In the deduction process, we will show that the low
 176 computation complexity and minimal memory footprint of NTT algorithm are based on
 177 the unique properties of twiddle factors, which can be generalized as four items :

$$\begin{aligned} \text{Sum property: } & \sum_{j=0}^{N-1} \omega_N^{kj} = \frac{(\omega_N^k)^N - 1}{\omega_N^k - 1} = \frac{(\omega_N^N)^k - 1}{\omega_N^k - 1} = 0 \quad \text{where } k \nmid N \\ \text{Binary property: } & \omega_N^{k+N/2} = -\omega_N^k \\ \text{Periodicity property: } & \omega_N^{k+N} = \omega_N^k \\ \text{Elimination property: } & \omega_{dN}^{dk} = \omega_N^k \end{aligned} \tag{4}$$

179 It is easy to see that the Binary property can be derived from Elimination property and
 180 the $2N$ -th roots of unity ϕ_{2N} also has similar properties.

181 2.2 Scalability of NTT Architecture

182 2.2.1 Dimensions of Scalability

183 Our scalable in-place NTT multiplication architecture considers four dimensions of scal-
 184 ability: length of data vector, different modulus, number of parallel butterfly units and
 185 arbitrary radix, which are denoted as N , q , d , R , respectively. While the configuration for N
 186 and q can be easily obtained, supporting different radix and multiple parallel butterfly units
 187 becomes a tough problem owing to the complex memory access in every stage. In fact, the
 188 interconnect network is an important component of NTT hardware, which guarantees the
 189 data points to be fetched and stored without conflicts so that no queues and reordering are
 190 needed. For example, [XHY⁺20] increases the number of parallel butterfly units to achieve
 191 high throughput in radix-2 NTT. For correct memory access, it proposes a permutation
 192 network, which needs six configuration modes and consumes more hardware resources. To
 193 reduce these overheads, we propose a more efficient conflict-free memory mapping scheme.
 194 This scheme is also valid for parallel non-radix-2 NTT hardware design.

195 **Interleaved memory system.** If the radix- R in-place NTT contains d butterfly units,
 196 $R \times d$ memory access should be performed in parallel. The memory bandwidth can be
 197 increased by partitioning the memory into $R \times d$ independent banks, which is referred
 198 to an interleaved (matched) memory system [TJS03]. To distribute data points over
 199 the interleaved memory system without conflict is a more difficult and universe problem
 200 compared to that of unmatched memory system. Because multiple data points can be
 201 stored into a single address by increasing the row-bandwidth in unmatched memory system.
 202 Its storage structure can be straightforwardly obtained according to the mapping scheme
 203 of interleaved memory system. Thus we focus on the memory mapping scheme for in-place
 204 NTT with interleaved memory system in this article.

2.2.2 Temporal and Spatial Conflicts

205 **Temporal conflict.** In pipelined NTT architecture, temporal conflict occurs when the
207 read operation of stage k is performed before the write operation of stage $k - 1$ [CMV⁺15].
208 Figure 1 provides an example of 16-points in-place radix-2 NTT for this read-before-write
(RBW) conflict. In pipelined radix-2 in-place NTT architecture, the time between the last

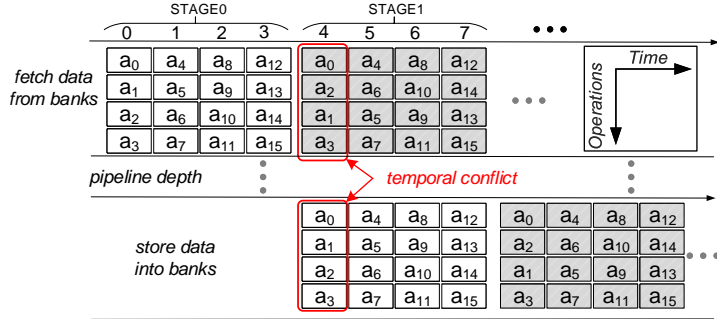


Figure 1: The temporal conflict in pipelined in-place NTT architecture.

209 two stages is the point at which conflict is most likely to occur. To avoid this conflict and
210 achieve 100% usage of NTT processor, the pipeline depth ought to meet the condition:
211 $\frac{N}{4d} \geq \text{pipeline depth}$. This condition will become more stringent when considering the
212 higher radix NTT. Fortunately, the data vector size in PQC and FHE algorithm is from
213 hundreds to millions magnitude, so this condition can be met under normal situations.
214

215 **Spatial conflict.** In every stage of NTT computation, if multiple data points are mapped
216 onto the same bank, we need to perform several read or write operations on a single bank
217 address simultaneously, which results in the so-called spatial conflict. [Joh92] proposes a
218 memory mapping scheme for arbitrary in-place FFT hardware, which is described in Figure
219 2(a) taking 8 points radix-2 FFT as an example. However, [ZYC⁺20] and [XMX17] point

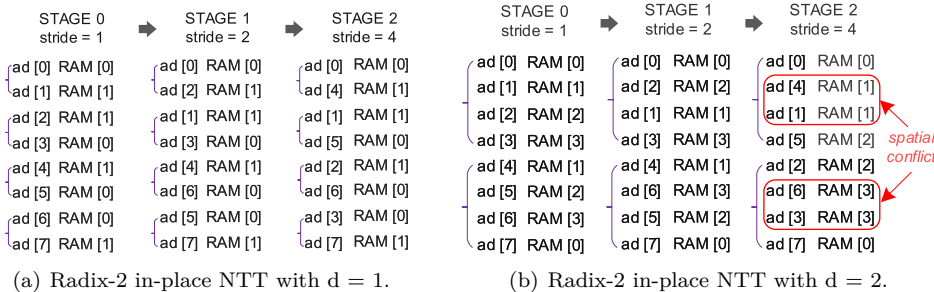


Figure 2: The spatial conflict in 8 points radix-2 in-place NTT.

219 out that this scheme is not suitable for the case when placing multiple butterfly units in
220 every stage. This spatial conflict is shown in Figure 2(b) using 8 points radix-2 FFT with
221 two butterfly units as an example. Instead of designing complex permutation networks as
222 [XHY⁺20], we will propose a general and simple scheme to solve this problem in section 4.
223

3 Radix-4 DIT NTT and DIF INTT

3.1 DIT Radix-4 NTT with Low Complexity

The pre-processing requires N modular multiplications for each input vector as equation 3 shows. Based on the tricks of [ZYC⁺20] [POG15], we can still avoid this process by merging the $2N$ -th roots of unity into every stage of Cooley-Tukey radix-4 DIT NTT algorithm. Thus, the number of modular multiplications is reduced from $(N \log_4 N) + 2N$ to $N \log_4 N$ in the proposed algorithm. Our derivation also follows the divide-and-conquer strategy in [Sto06], where the DFT is divided in time domain. Firstly, the pre-processing and the main NTT are written together as belows :

$$A_i = \sum_{j=0}^{N-1} a_j \phi_{2N}^j \omega_N^{ij} \bmod q \quad i = 0, 1, \dots, N-1 \quad (5)$$

Then, by splitting the summation into four coresidual groups according to the time domain index j , the equation 6 is transformed as :

$$\begin{aligned} A_i = & \sum_{j=0}^{N/4-1} a_{4j} \phi_{2N}^{4j} \omega_N^{i \cdot (4j)} + \sum_{j=0}^{N/4-1} a_{4j+1} \phi_{2N}^{4j+1} \omega_N^{i \cdot (4j+1)} + \\ & \sum_{j=0}^{N/4-1} a_{4j+2} \phi_{2N}^{4j+2} \omega_N^{i \cdot (4j+2)} + \sum_{j=0}^{N/4-1} a_{4j+3} \phi_{2N}^{4j+3} \omega_N^{i \cdot (4j+3)} \bmod q \\ & i = 0, 1, \dots, N-1 \end{aligned} \quad (6)$$

By leveraging the Elimination property of twiddle factor ω and ϕ , the equation 6 can be simplified as :

$$\begin{aligned} A_i = & \sum_{j=0}^{N/4-1} a_{4j} \phi_{N/2}^j \omega_{N/4}^{ij} + \omega_N^i \cdot \phi_{2N}^1 \cdot \sum_{j=0}^{N/4-1} a_{4j+1} \phi_{N/2}^j \omega_{N/4}^{ij} + \\ & \omega_N^{2i} \cdot \phi_{2N}^2 \cdot \sum_{j=0}^{N/4-1} a_{4j+2} \phi_{N/2}^j \omega_{N/4}^{ij} + \omega_N^{3i} \cdot \phi_{2N}^3 \cdot \sum_{j=0}^{N/4-1} a_{4j+3} \phi_{N/2}^j \omega_{N/4}^{ij} \bmod q \\ & i = 0, 1, \dots, N/4-1 \end{aligned} \quad (7)$$

For simplicity, let F_0, F_1, F_2 and F_3 denote the four summation items $\sum_{j=0}^{N/4-1} a_{4j} \phi_{N/2}^j \omega_{N/4}^{ij}$, $\sum_{j=0}^{N/4-1} a_{4j+1} \phi_{N/2}^j \omega_{N/4}^{ij}$, $\sum_{j=0}^{N/4-1} a_{4j+2} \phi_{N/2}^j \omega_{N/4}^{ij}$, $\sum_{j=0}^{N/4-1} a_{4j+3} \phi_{N/2}^j \omega_{N/4}^{ij}$, respectively. Then, the equation 7 is written as :

$$A_i = F_0 + \omega_N^i \cdot \phi_{2N}^1 \cdot F_1 + \omega_N^{2i} \cdot \phi_{2N}^2 \cdot F_2 + \omega_N^{3i} \cdot \phi_{2N}^3 \cdot F_3 \quad i = 0, 1, \dots, N/4-1 \quad (8)$$

Obviously, by applying the Periodicity property of twiddle factor, the other three equations can be obtained as:

$$\begin{aligned} A_{i+N/4} &= F_0 + \omega_N^i \cdot \omega_4^1 \cdot \phi_{2N}^1 \cdot F_1 + \omega_N^{2i} \cdot \omega_4^2 \cdot \phi_{2N}^2 \cdot F_2 + \omega_N^{3i} \cdot \omega_4^3 \cdot \phi_{2N}^3 \cdot F_3 \\ A_{i+2N/4} &= F_0 + \omega_N^i \cdot \omega_4^2 \cdot \phi_{2N}^1 \cdot F_1 + \omega_N^{2i} \cdot (\omega_4^2)^2 \cdot \phi_{2N}^2 \cdot F_2 + \omega_N^{3i} \cdot (\omega_4^2)^3 \cdot \phi_{2N}^3 \cdot F_3 \\ A_{i+3N/4} &= F_0 + \omega_N^i \cdot \omega_4^3 \cdot \phi_{2N}^1 \cdot F_1 + \omega_N^{2i} \cdot (\omega_4^3)^2 \cdot \phi_{2N}^2 \cdot F_2 + \omega_N^{3i} \cdot (\omega_4^3)^3 \cdot \phi_{2N}^3 \cdot F_3 \end{aligned} \quad (9)$$

$$i = 0, 1, \dots, N/4-1$$

247 According to the Sum property and Binary property, we can derive that $\omega_4^3 = -\omega_4^1$,
248 $\omega_4^2 = -\omega_4^0 = -1$. So we can express the equation 8 and 9 in the form of matrix as belows:

$$\begin{bmatrix} A_i \\ A_{i+N/4} \\ A_{i+2N/4} \\ A_{i+3N/4} \end{bmatrix} = \left(\begin{bmatrix} 1 & 1 & 1 & 1 \\ 1 & \omega_4^1 & -1 & -\omega_4^1 \\ 1 & -1 & 1 & -1 \\ 1 & -\omega_4^1 & -1 & \omega_4^1 \end{bmatrix} \times \begin{bmatrix} F_0 \\ F_1 \\ F_2 \\ F_3 \end{bmatrix} \right) \cdot \begin{bmatrix} 1 \\ \omega_N^i \cdot \phi_{2N}^1 \\ \omega_N^{2i} \cdot \phi_{2N}^2 \\ \omega_N^{3i} \cdot \phi_{2N}^3 \end{bmatrix} \quad i = 0, 1, \dots, N/4-1 \quad (10)$$

249 Note that F_0 , F_1 , F_2 and F_3 are actually the four $N/4$ -points NTTs, essentially similar
250 to equation 6. By adopting this divide-and-conquer strategy recursively until $\frac{N}{4}$ 4-points,
251 we can obtain the radix-4 NTT algorithm. Furthermore, by merging the powers of N -th
252 roots of unity ω_N and $2N$ -th roots of unity ϕ_{2N} in equation 10, we can obtain that:
253

$$\begin{bmatrix} A_i \\ A_{i+N/4} \\ A_{i+2N/4} \\ A_{i+3N/4} \end{bmatrix} = \left(\begin{bmatrix} 1 & 1 & 1 & 1 \\ 1 & \omega_4^1 & -1 & -\omega_4^1 \\ 1 & -1 & 1 & -1 \\ 1 & -\omega_4^1 & -1 & \omega_4^1 \end{bmatrix} \times \begin{bmatrix} F_0 \\ F_1 \\ F_2 \\ F_3 \end{bmatrix} \right) \cdot \begin{bmatrix} 1 \\ \phi_{2N}^{2i+1} \\ \phi_{2N}^{2(2i+1)} \\ \phi_{2N}^{3(2i+1)} \end{bmatrix} \quad i = 0, 1, \dots, N/4-1 \quad (11)$$

254 Up to now, we just need to precompute the powers of ϕ_{2N} for storage, eliminating the
255 pre-processing of $2N$ modular multiplication completely.
256

3.2 DIF Radix-4 INTT with Low Complexity

257 By merging the scale factor N^{-1} and powers of $2N$ -th roots of unity ϕ_{2N}^{-1} into every stage,
258 the number of modular multiplications in radix-4 INTT algorithm can be reduced from
259 $N \log_4 N + N$ to $N \log_4 N$ [ZYC⁺20] [POG15]. At this time, we will adopt the strategy
260 in [GS66], where the DFT is divided in frequency domain and it turns out the so-called
261 Gentleman-Sande Butterfly. At the very beginning, the post-processing and the main
262 INTT are written together as:
263

$$264 \quad a_i = N^{-1} \cdot \phi_{2N}^{-i} \cdot \sum_{j=0}^{N-1} A_j \omega_N^{-ij} \bmod q \quad i = 0, 1, \dots, N-1 \quad (12)$$

265 According to the index i , we can split the summation into four consecutive groups with
266 the same size $N/4$. Then, the equation 12 is transformed as:
267

$$\begin{aligned} a_i &= N^{-1} \cdot (\phi_{2N}^{-i} \cdot \sum_{j=0}^{N/4-1} A_j \phi_{2N}^{-j} \omega_N^{-ij} + \phi_{2N}^{-i} \cdot \sum_{j=N/4}^{2N/4-1} A_j \omega_N^{-ij} + \\ &\quad \phi_{2N}^{-i} \cdot \sum_{j=2N/4}^{3N/4-1} A_j \omega_N^{-ij} + \phi_{2N}^{-i} \cdot \sum_{j=3N/4}^{N-1} A_j \omega_N^{-ij}) \bmod q \quad i = 0, 1, \dots, N-1 \end{aligned} \quad (13)$$

268 Based on the Periodicity and Binary property of twiddle factor, we can put the four
269 summation items into the same range $[0, N/4 - 1]$:

$$\begin{aligned} a_i &= N^{-1} \cdot (\phi_{2N}^{-i} \cdot \sum_{j=0}^{N/4-1} A_j \omega_N^{-ij} + \phi_{2N}^{-i} \cdot \sum_{j=0}^{N/4-1} A_{j+N/4} \omega_N^{-i \cdot (j+N/4)} + \\ &\quad \phi_{2N}^{-i} \cdot \sum_{j=0}^{N/4-1} A_{j+2N/4} \omega_N^{-i \cdot (j+2N/4)} + \phi_{2N}^{-i} \cdot \sum_{j=0}^{N/4-1} A_{j+3N/4} \omega_N^{-i \cdot (j+3N/4)}) \bmod q \\ &\quad i = 0, 1, \dots, N/4 - 1 \end{aligned} \quad (14)$$

²⁷¹ Because of the Elimination property, the equation 14 can be simplified as:

$$\begin{aligned} a_i &= N^{-1} \cdot (\phi_{2N}^{-i} \cdot \sum_{j=0}^{N/4-1} A_j \omega_N^{-ij} + \phi_{2N}^{-i} \cdot \omega_4^{-i} \cdot \sum_{j=0}^{N/4-1} A_{j+N/4} \omega_N^{-ij} + \\ &\quad \phi_{2N}^{-i} \cdot \omega_4^{-2i} \cdot \sum_{j=0}^{N/4-1} A_{j+2N/4} \omega_N^{-ij} + \phi_{2N}^{-i} \cdot \omega_4^{-3i} \cdot \sum_{j=0}^{N/4-1} A_{j+3N/4} \omega_N^{-ij}) \bmod q \\ &\quad i = 0, 1, \dots, N/4 - 1 \end{aligned} \tag{15}$$

²⁷² Note that the factors ω_4^{-i} , ω_4^{-2i} , ω_4^{-3i} can be classified into four cases according to the
²⁷³ coresidual groups of index i:

$$\begin{aligned} \omega_4^{-i} &= \begin{cases} 0 & i = 4r \\ \omega_4^{-1} & i = 4r + 1 \\ -1 & i = 4r + 2 \\ -\omega_4^{-1} & i = 4r + 3 \end{cases} \quad \omega_4^{-2i} = \begin{cases} 1 & i = 4r \\ -1 & i = 4r + 1 \\ 1 & i = 4r + 2 \\ -1 & i = 4r + 3 \end{cases} \quad \omega_4^{-3i} = \begin{cases} 0 & i = 4r \\ \omega_4^{-1} & i = 4r + 1 \\ -1 & i = 4r + 2 \\ -\omega_4^{-1} & i = 4r + 3 \end{cases} \\ &\quad r = 0, 1, \dots, N/4 - 1 \end{aligned} \tag{16}$$

²⁷⁵ As a result, the equation 16 can be grouped into four parts based on the coresidual groups
²⁷⁶ of index i, correspondingly. With the Elimination property of twiddle factor, the first part
²⁷⁷ can be further written as:

$$\begin{aligned} a_{4i} &= (\frac{N}{4})^{-1} \cdot (\frac{1}{4} \cdot \phi_{N/2}^{-i} \cdot \sum_{j=0}^{N/4-1} A_j \omega_{N/4}^{-ij} + \frac{1}{4} \cdot \phi_{N/2}^{-i} \cdot \sum_{j=0}^{N/4-1} A_{j+N/4} \omega_{N/4}^{-ij} + \\ &\quad \frac{1}{4} \cdot \phi_{N/2}^{-i} \cdot \sum_{j=0}^{N/4-1} A_{j+2N/4} \omega_{N/4}^{-ij} + \frac{1}{4} \cdot \phi_{N/2}^{-i} \cdot \sum_{j=0}^{N/4-1} A_{j+3N/4} \omega_{N/4}^{-ij}) \bmod q \\ &\quad i = 0, 1, \dots, N/4 - 1 \end{aligned} \tag{17}$$

²⁷⁹ For simplicity, let G_0, G_1, G_2, G_3 denote the four summation items, respectively.

$$G_m = (\frac{N}{4})^{-1} \cdot \phi_{N/2}^{-i} \cdot \sum_{j=0}^{N/4-1} \frac{1}{4} A_{j+mN/4} \phi_{N/2}^{-i} \omega_{N/4}^{-ij} \quad m = 0, 1, 2, 3 \tag{18}$$

²⁸² Thus, the four parts of equation 16 can be expressed as:

$$\begin{aligned} a_{4i} &= G_0 + G_1 + G_2 + G_3 \\ a_{4i+1} &= \phi_{2N}^{-1} \cdot \omega_N^{-j} \cdot (G_0 + \omega_4^{-1} G_1 + \omega_4^{-2} G_2 + \omega_4^{-3} G_3) \\ a_{4i+2} &= \phi_{2N}^{-2} \cdot \omega_N^{-2j} \cdot [G_0 + \omega_4^{-2} G_1 + (\omega_4^{-2})^2 G_2 + (\omega_4^{-3})^2 G_3] \\ a_{4i+3} &= \phi_{2N}^{-3} \cdot \omega_N^{-3j} \cdot [G_0 + \omega_4^{-3} G_1 + (\omega_4^{-2})^3 G_2 + (\omega_4^{-3})^3 G_3] \\ &\quad i = 0, 1, \dots, N/4 - 1 \end{aligned} \tag{19}$$

²⁸⁴ With the Sum and Binary property, we can derive that $\omega_4^{-3} = -\omega_4^{-1}$, $\omega_4^{-2} = -\omega_4^0 = -1$.
²⁸⁵ Thus, the equation 20 is further expressed in matrix form:

$$\begin{aligned} \begin{bmatrix} a_{4i} \\ a_{4i+1} \\ a_{4i+2} \\ a_{4i+3} \end{bmatrix} &= \left(\begin{bmatrix} G_0 \\ G_1 \\ G_2 \\ G_3 \end{bmatrix} \cdot \begin{bmatrix} 1 \\ \omega_N^{-j} \cdot \phi_{2N}^{-1} \\ \omega_N^{-2j} \cdot \phi_{2N}^{-2} \\ \omega_N^{-3j} \cdot \phi_{2N}^{-3} \end{bmatrix} \right) \times \begin{bmatrix} 1 & 1 & 1 & 1 \\ 1 & \omega_4^{-1} & -1 & -\omega_4^{-1} \\ 1 & -1 & 1 & -1 \\ 1 & -\omega_4^{-1} & -1 & \omega_4^{-1} \end{bmatrix} \\ &\quad i = 0, 1, \dots, N/4 - 1 \end{aligned} \tag{20}$$

287 In this way, the N -points INTT can be divided into four $\frac{N}{4}$ -points INTTs. By adopting
 288 this strategy recursively until $\frac{N}{4}$ 4-points INTTs, we can obtain the DIF radix-4 INTT
 289 algorithm. Note that the scale factor is also merged into each stage and the equation 20
 290 can be further written as:

$$\begin{bmatrix} a_{4i} \\ a_{4i+1} \\ a_{4i+2} \\ a_{4i+3} \end{bmatrix} = \left(\begin{bmatrix} G_0 \\ G_1 \\ G_2 \\ G_3 \end{bmatrix} \cdot \begin{bmatrix} 1 \\ \phi_{2N}^{-(2j+1)} \\ \phi_{2N}^{-2(2j+1)} \\ \phi_{2N}^{-3(2j+1)} \end{bmatrix} \right) \times \begin{bmatrix} 1 & 1 & 1 & 1 \\ 1 & \omega_4^{-1} & -1 & -\omega_4^{-1} \\ 1 & -1 & 1 & -1 \\ 1 & -\omega_4^{-1} & -1 & \omega_4^{-1} \end{bmatrix} \quad (21)$$

$i = 0, 1, \dots, N/4 - 1$

292 By now, we just need to precalculate the powers of $2N$ -th roots of unity ϕ_{2N}^{-1} for storage
 293 and the post-processing of N -modular multiplication is removed completely.

3.3 Improvement with Divide and Schedule Method

295 In this section, a versatile schedule method is utilized to reduce the number of modular
 296 multiplications and modular additions/subtractions by 20% and 30%, respectively. There-
 297 after, the complete radix-4 DIT NTT algorithm and radix-4 DIF INTT algorithm with
 298 low complexity are presented.

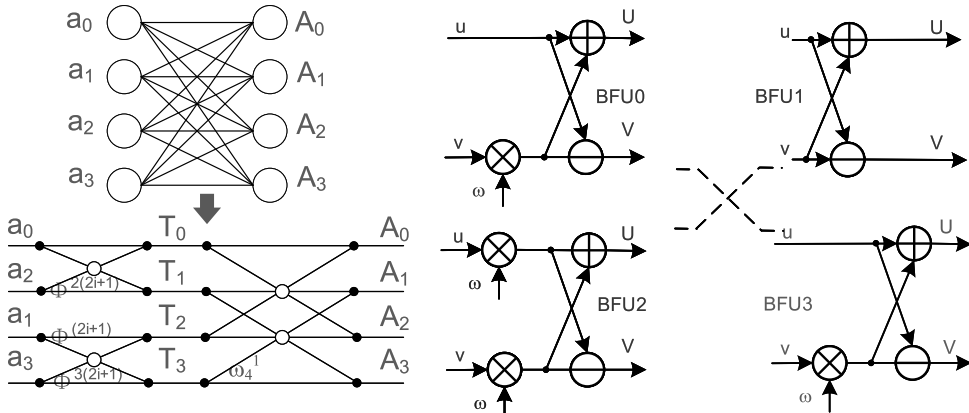


Figure 3: The radix-4 Cookley-Tukey butterfly unit.

299
 300 **Divide and schedule in radix-4 Cooley-Tukey butterfly.** When directly calculating
 301 the equation 11, it will take 5 modular multiplications, 6 modular additions and 6 modular
 302 subtractions. However, based on the divide-and-conquer idea, this computation complexity
 303 can be further reduced [HT96]. It is easy to see that some immediate results can be
 304 reused when calculating the radix-4 butterfly operation. Thus, we schedule the matrix
 305 multiplication into two-layer operations as belows:

$$\begin{aligned}
 T_0 &= (F_0 + F_2 \cdot \phi_{2N}^{2(2i+1)}) & A_i &= T_0 + T_2 \\
 T_1 &= (F_0 - F_2 \cdot \phi_{2N}^{2(2i+1)}) & A_{i+N/4} &= (T_1 + T_3 \cdot \omega_4^1) \\
 T_2 &= (F_1 \cdot \phi_{2N}^{2i+1} + F_3 \cdot \phi_{2N}^{3(2i+1)}) & A_{i+2N/4} &= (T_0 - T_2) \\
 T_3 &= (F_1 \cdot \phi_{2N}^{2i+1} - F_3 \cdot \phi_{2N}^{3(2i+1)}) & A_{i+3N/4} &= (T_1 - T_3 \cdot \omega_4^1)
 \end{aligned} \quad (22)$$

306 At this time, the radix-4 butterfly unit operation is reduced to 4 modular multiplications
 307 and 4 modular additions and 4 modular subtractions, which results in the two-layer

Algorithm 2 Radix-4 DIT Iterative NTT Algorithm

Input: \mathbf{a} denotes a vector of length N , q is modulus and ϕ_{2N} is $2N$ -th primitive roots of unity. ω_4^1 is 4-th primitive roots of unity.

Output: $\mathbf{A} = \text{DIT_NTT}(\mathbf{a})$

```

1:  $\mathbf{A} \leftarrow \text{bit reverse}(\mathbf{a})$ 
2: for  $p = 0$  to  $\log_4 N - 1$  do
3:    $J \leftarrow 4^p$ 
4:    $\omega_m \leftarrow \phi_{2N}^{N/(4J)}$ 
5:   for  $k = 0$  to  $N/(4J) - 1$  do
6:     for  $j = 0$  to  $J - 1$  do
7:        $T_0 \leftarrow (a_{4kJ+j} + a_{4kJ+j+2J} \cdot \omega_m^{2(2j+1)}) \bmod q$ 
8:        $T_1 \leftarrow (a_{4kJ+j} - a_{4kJ+j+2J} \cdot \omega_m^{2(2j+1)}) \bmod q$ 
9:        $T_2 \leftarrow (a_{4kJ+j+J} \cdot \omega_m^{2j+1} + a_{4kJ+j+3J} \cdot \omega_m^{3(2j+1)}) \bmod q$ 
10:       $T_3 \leftarrow (a_{4kJ+j+J} \cdot \omega_m^{2j+1} - a_{4kJ+j+3J} \cdot \omega_m^{3(2j+1)}) \bmod q$ 
11:       $A_{4kJ+j} \leftarrow (T_0 + T_2) \bmod q$ 
12:       $A_{4kJ+j+J} \leftarrow (T_1 + T_3 \cdot \omega_4^1) \bmod q$ 
13:       $A_{4kJ+j+2J} \leftarrow (T_0 - T_2) \bmod q$ 
14:       $A_{4kJ+j+3J} \leftarrow (T_1 - T_3 \cdot \omega_4^1) \bmod q$ 
15:    end for
16:   end for
17: end for
18: return  $\mathbf{A}$ 

```

309 Cooley-Tukey butterfly unit. The Figure 3 can depict this change intuitively and presents
 310 the detailed architecture. As a result, the complete two-layer radix-4 DIT NTT with low
 311 complexity is demonstrated in algorithm 2.

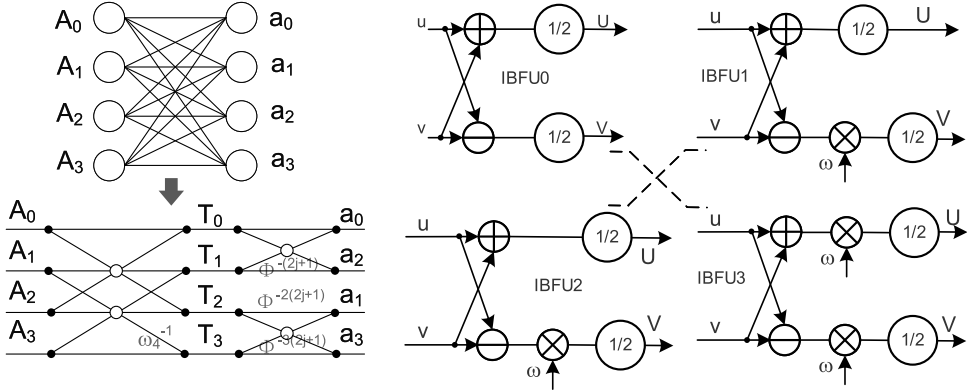
312 **Divide and schedule in radix-4 Gentleman-Sande butterfly.** Similar to radix-4
 313 NTT, the complexity in radix-4 INTT butterfly operation can also be further reduced.
 314 Using straightforward method to compute the equation 20 still requires 5 modular mul-
 315 tiplications, 6 modular additions and 6 modular subtractions. Thus, by scheduling the
 316 matrix multiplication to reuse the immediate result, we obtain that:

$$\begin{aligned}
 T_0 &= F_0 + F_2 & a_{4i} &= T_0 + T_2 \\
 T_1 &= F_0 - F_2 & a_{4i+1} &= (T_1 + T_3) \cdot \phi_{2N}^{-(2j+1)} \\
 T_2 &= F_1 + F_3 & a_{4i+2} &= (T_0 - T_2) \cdot \phi_{2N}^{-2(2j+1)} \\
 T_3 &= (F_1 - F_3) \cdot \omega_4^{-1} & a_{4i+3} &= (T_1 - T_3) \cdot \phi_{2N}^{-3(2j+1)}
 \end{aligned} \tag{23}$$

318 In this way, we just need 4 modular multiplications, 4 modular multiplications and 4
 319 modular additions and 4 modular subtractions, which results in the two-layer Gentleman-
 320 Sande butterfly unit. The Figure 4 also presents the changes and detailed architecture.
 321 Since the ω_4^1 and ω_4^{-1} are constants, the multiplication in BFU3 and IBFU2 can be
 322 alternatively implemented with a series of additions and shifts. So far, the complete
 323 two-layer radix-4 DIF INTT with low complexity is demonstrated in algorithm 3.

3.4 Avoiding Bit-reversed Cost and Reducing Memory Footprint

324 When straightly performing the classic in-place DIT NTT and DIF INTT as [ZYC⁺²⁰]
 325 [XHY⁺²⁰] [MKÖ^{+20b}], bit-reversed operation is required at the very beginning of NTT
 326 and ending of INTT, respectively. Because the classic DIT NTT receives the input vector
 327 with bit-reversed order and produces the output vector with natural order. The classic
 328 DIF INTT is contrary to the orientation of DIT NTT. [POG15] [XL21] [CG99] avoid
 329 the bit-reversed operation for radix-2 DIT NTT and DIF INTT by rearranging the loop
 330 structure and storage structure of twiddle factors. In this section, we will generalize
 331 this bit-reversed issue for arbitrary radix DIT NTT and DIF INTT and propose the

**Figure 4:** The radix-4 Gentleman-Sande butterfly unit.**Algorithm 3** Radix-4 DIF Iterative INTT Algorithm

Input: \mathbf{a} denotes a vector of length N , q is modulus and ϕ_{2N}^{-1} is inverse element of $2N$ -th primitive roots of unity. ω_4^{-1} is inverse element of 4-th primitive roots of unity.

Output: $\mathbf{A} = \text{DIF_INTT}(\mathbf{a})$

```

1: for  $p = \log_4 N - 1$  to 0 do
2:    $J \leftarrow 4^p$ 
3:    $\omega_m \leftarrow \phi_{2N}^{-N/(4J)}$ 
4:   for  $k = 0$  to  $N/(4J) - 1$  do
5:     for  $j = 0$  to  $J - 1$  do
6:        $T_0 \leftarrow \frac{1}{2} \cdot (a_{4kJ+j} + a_{4kJ+j+2J}) \bmod q$ 
7:        $T_1 \leftarrow \frac{1}{2} \cdot (a_{4kJ+j} - a_{4kJ+j+2J}) \bmod q$ 
8:        $T_2 \leftarrow \frac{1}{2} \cdot (a_{4kJ+j+J} + a_{4kJ+j+3J}) \bmod q$ 
9:        $T_3 \leftarrow \frac{1}{2} \cdot (a_{4kJ+j+J} - a_{4kJ+j+3J}) \cdot \omega_4^{-1} \bmod q$ 
10:       $A_{4kJ+j} \leftarrow \frac{1}{2} \cdot (T_0 + T_2) \bmod q$ 
11:       $A_{4kJ+j+J} \leftarrow \frac{1}{2} \cdot (T_1 + T_3) \cdot \omega_m^{-(2j+1)} \bmod q$ 
12:       $A_{4kJ+j+2J} \leftarrow \frac{1}{2} \cdot (T_0 - T_2) \cdot \omega_m^{-2(2j+1)} \bmod q$ 
13:       $A_{4kJ+j+3J} \leftarrow \frac{1}{2} \cdot (T_1 - T_3) \cdot \omega_m^{-3(2j+1)} \bmod q$ 
14:    end for
15:   end for
16: end for
17:  $\mathbf{A} \leftarrow \text{bit reverse}(\mathbf{A})$ 
18: return  $\mathbf{A}$ 

```

333 bit-reversed-free radix-4 DIT NTT and DIF INTT algorithm, respectively. We use the
 334 notation NR (RN) as belows to represent that the input vector is received in natural
 335 (bit-reversed) order and the output vector is produced in bit-reversed (natural) order. In
 336 addition, we will show how the memory footprint can be reduced by reusing the twiddle
 337 factors of forward radix-2/4 NTT in the inverse radix-2/4 NTT.

338 **3.4.1 Proposed DIT-NR Radix-4 NTT**

339 In DIT NTT, the bit-reversed-free trait indicates that the input vector is received in
 340 natural order and the output vector is produced in bit-reversed order, which is opposite to
 341 the classic DIT NTT. [CG99] obtains the radix-2 bit-reversed-free DIT NTT by changing
 342 the loop structure and the storage method of twiddle factors. Inspired by this work,
 343 we derive the radix-4 bit-reversed-free DIT NTT algorithm. Based on this derivation,
 344 the bit-reversed operation in arbitrary radix NTT can be removed. This optimization
 345 technique is achieved by three important observations as belows:

- 346 (1) In analogy with classic DIF INTT algorithm, the address with natural order in DIT
 347 NTT can be generated by just reversing the first loop.
 348 (2) To still obtain the correct results after reversing the first loop, the generation of
 349 twiddle factors are required to rearranged accordingly.
 350 (3) After performing the operation in (1), the iterative principle of index j and k in
 351 algorithm 2 will exactly exchange with each other.

352 As a result, the arrangement of twiddle factors in item (2) can be realized with three steps
 353 based on item (3). The first step is to move the place of generating twiddle factors from
 354 the innermost loop j to the middle loop k. The second step is to replace the index j in
 355 exponential position of twiddle factors in algorithm 2 with bit-reversed index k. The final
 356 step is to replace the powers $N/(4J)$ in algorithm 2 line 4 with powers J . It is worth to
 357 mention that this method can also be applied in DIT NTT of other radix to avoid the
 358 bit-reversed cost. The detailed changes in terms of the generation of twiddle factors can
 359 be described in equation 24.

$$\begin{aligned} \phi_{2N}^{N/(4J)} &\Rightarrow \phi_{2N}^J & \omega_m^{2j+1} &\Rightarrow \omega_m^{2\text{bit-reversed}(k)+1} \\ \omega_m^{2(2j+1)} &\Rightarrow \omega_m^{2 \cdot (2\text{bit-reversed}(k)+1)} & \omega_m^{3(2j+1)} &\Rightarrow \omega_m^{3 \cdot (2\text{bit-reversed}(k)+1)} \end{aligned} \quad (24)$$

361 In the hardware implementation, the twiddle factors are actually precomputed and stored
 362 in the ROM. Hence, we propose the complete bit-reversed-free radix-4 DIT NTT in
 363 algorithm 4 along with the method of precomputing twiddle factors. Figure 5(a) presents
 364 the corresponding 16-points dataflow of radix-4 DIT-NR NTT where the input vector is
 365 accepted in natural order and the output vector is produced in bit-reversed order. The
 366 lines with red and yellow color represent the first-round butterfly operation in stage 0 and
 367 stage 1, respectively.

368 3.4.2 Proposed DIF-RN Radix-4 INTT

369 In DIF INTT, the bit-reversed-free trait indicates that the input vector is received in
 370 bit-reversed order and the output vector is produced in natural order, which is also opposite
 371 to the classic DIF INTT. Based on DIT-NR NTT, we can obtain the DIF-RN INTT with
 372 a direct method by just reversing the fisrt loop in algorithm 3 line 1 and replacing the
 373 twiddle factor in equation 24 with its inverse element. Nevertheless, this method cannot
 374 lead to a perfect implementation in terms of memory footprint. As shown in the reference

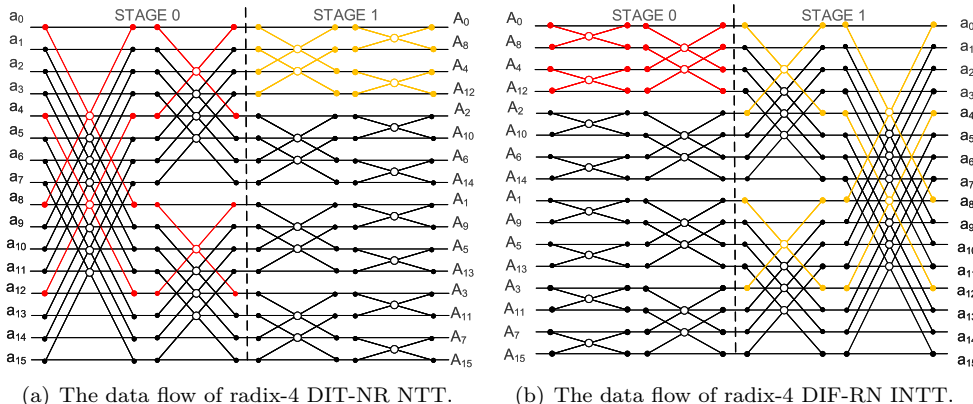


Figure 5: The data flow of 16 points radix-4 NTT/INTT.

Algorithm 4 Radix-4 DIT-NR NTT Algorithm

Input: a denotes a vector of length N , q is modulus and ϕ_{2N} is $2N$ -th primitive roots of unity. ω_4^1 is 4-th primitive roots of unity.

Output: $A = \text{DIT-NR NTT}(a)$

```

1: Precompute the twiddle factors:
2: for  $p = \log_4 N - 1$  to 0 do
3:    $J \leftarrow 4^p$ 
4:    $\omega_m \leftarrow \phi_{2N}^J$ 
5:   for  $k = 0$  to  $N/(4J) - 1$  do
6:      $\text{wa1\_ROM.append } [\omega_m^{2\text{bit-reversed}(k)+1}]$ 
7:      $\text{wa2\_ROM.append } [\omega_m^{2 \cdot (2\text{bit-reversed}(k)+1)}]$ 
8:      $\text{wa3\_ROM.append } [\omega_m^{3 \cdot (2\text{bit-reversed}(k)+1)}]$ 
9:   end for
10: end for
11: Perform the radix-4 DIT-NR NTT:
12: for  $p = \log_4 N - 1$  to 0 do
13:    $J \leftarrow 4^p$ 
14:    $r \leftarrow 0$ 
15:   for  $k = 0$  to  $N/(4J) - 1$  do
16:      $w_1 \leftarrow \text{wa1\_ROM}[r]$ 
17:      $w_2 \leftarrow \text{wa2\_ROM}[r]$ 
18:      $w_3 \leftarrow \text{wa3\_ROM}[r]$ 
19:      $r \leftarrow r + 1$ 
20:     for  $j = 0$  to  $J - 1$  do
21:        $T_0 \leftarrow (a_{4kJ+j} + a_{4kJ+j+2J} \cdot \omega_2) \bmod q$ 
22:        $T_1 \leftarrow (a_{4kJ+j} - a_{4kJ+j+2J} \cdot \omega_2) \bmod q$ 
23:        $T_2 \leftarrow (a_{4kJ+j+J} \cdot \omega_1 + a_{4kJ+j+3J} \cdot \omega_3) \bmod q$ 
24:        $T_3 \leftarrow (a_{4kJ+j+J} \cdot \omega_1 - a_{4kJ+j+3J} \cdot \omega_3) \bmod q$ 
25:        $A_{4kJ+j} \leftarrow (T_0 + T_2) \bmod q$ 
26:        $A_{4kJ+j+J} \leftarrow (T_1 + T_3 \cdot \omega_4^1) \bmod q$ 
27:        $A_{4kJ+j+2J} \leftarrow (T_0 - T_2) \bmod q$ 
28:        $A_{4kJ+j+3J} \leftarrow (T_1 - T_3 \cdot \omega_4^1) \bmod q$ 
29:     end for
30:   end for
31: end for
32: return  $A$ 

```

375 software implementation of Kyber from NIST, the twiddle factors in radix-2 DIF INTT
 376 can reuse the twiddle factors of radix-2 DIT INTT by leveraging the Binary property:
 377 $\phi_{2N}^N = -1 \bmod q \Rightarrow \phi_{2N}^{-i} = -\phi_{2N}^N \cdot \phi_{2N}^{-i} \bmod q = -\phi_{2N}^{N-i} \bmod q$. In this section, we show
 378 that the twiddle factors in radix-4 DIT-NR NTT can also be reused in radix-4 DIF-RN
 379 INTT by making full use of the properties of twiddle factors and suitable schedule. Firstly,
 380 we derive three tricks shown in equation 25 from the Binary and Elimination property of
 381 twiddle factors:

$$\begin{aligned}
 \phi_{2N}^{-i} \bmod q &= \phi_{2N}^{-N/2} \cdot \phi_{2N}^{N/2-i} \bmod q = \omega_4^{-1} \cdot \phi_{2N}^{N/4-i} \bmod q = -\omega_4^1 \cdot \phi_{2N}^{N/2-i} \bmod q \\
 \phi_{2N}^{-i} \bmod q &= -\phi_{2N}^N \cdot \phi_{2N}^{N-i} \bmod q = -\phi_{2N}^{N-i} \bmod q \\
 \phi_{2N}^{-i} \bmod q &= \phi_{2N}^{-3N/2} \cdot \phi_{2N}^{3N/2-i} \bmod q = -\phi_{2N}^{-N/2} \cdot \phi_{2N}^{3N/2-i} \bmod q \\
 &= -\omega_4^{-1} \cdot \phi_{2N}^{3N/2-i} \bmod q = \omega_4^1 \cdot \phi_{2N}^{3N/2-i} \bmod q
 \end{aligned} \tag{25}$$

383 Then, we apply these three tricks into equation 24 to obtain the inverse twiddle factor in
 384 algorithm 3 as belows:

$$\begin{aligned}
 \omega_m^{-(2j+1)} &\Rightarrow -\omega_4^1 \cdot \omega_m^{N/2-[2\text{bit-reversed}(k)+1]} \\
 \omega_m^{-2(2j+1)} &\Rightarrow -\omega_m^{N-[2 \cdot (2\text{bit-reversed}(k)+1)]} \\
 \omega_m^{-3(2j+1)} &\Rightarrow \omega_4^1 \cdot \omega_m^{3N/2-[3 \cdot (2\text{bit-reversed}(k)+1)]}
 \end{aligned} \tag{26}$$

386 Note that the factor ω_4^1 can be scheduled to multiply with ω_4^{-1} in algorithm 3 line 9. So
 387 applying the equation 26 into the two-layer butterfly operation of algorithm 3 will not
 388 increase the original complexity. To this end, we can reuse the twiddle factors generated
 389 in algorithm 4, which turns out the complete bit-reversed-free DIF INTT algirthm 5. As a
 390 result, the bit-reversed-free radix-4 Gentleman Sande butterfly unit can be obtained by
 391 just exchanging the position of IBFU0 with IBFU2 and swapping the two operands of
 392 modular subtracter in Figure 4. Figure 5(b) presents the corresponding 16-points dataflow
 393 of radix-4 DIF-RN INTT where the input vector are accepted in bit-reversed order and
 394 the output vector are produced in natural order. The lines with red and yellow color also
 represent the first-round butterfly operation in stage 0 and stage 1, respectively.

Algorithm 5 Radix-4 DIF-RN INTT Algorithm

Input: a denotes a vector of length N , q is modulus and $\omega a1_ROM$, $\omega a2_ROM$, $\omega a3_ROM$ are three arrays generated by algorithm 4.

Output: $A = \text{DIF-RN INTT}(a)$

```

1: for  $p = 0$  to  $\log_4 N - 1$  do
2:    $J \leftarrow 4^p$ 
3:    $r \leftarrow \frac{N-1}{3} - 1$ 
4:   for  $k = 0$  to  $N/(4J) - 1$  do
5:      $\omega_1 \leftarrow \omega a1\_ROM[r]$ 
6:      $\omega_2 \leftarrow \omega a2\_ROM[r]$ 
7:      $\omega_3 \leftarrow \omega a3\_ROM[r]$ 
8:      $r \leftarrow r - 1$ 
9:     for  $j = 0$  to  $J - 1$  do
10:       $T_0 \leftarrow \frac{1}{2} \cdot (a_{4kJ+j} + a_{4kJ+j+2J}) \bmod q$ 
11:       $T_1 \leftarrow \frac{1}{2} \cdot (a_{4kJ+j+2J} - a_{4kJ+j}) \cdot \omega_4^1 \bmod q$ 
12:       $T_2 \leftarrow \frac{1}{2} \cdot (a_{4kJ+j+J} + a_{4kJ+j+3J}) \bmod q$ 
13:       $T_3 \leftarrow \frac{1}{2} \cdot (a_{4kJ+j+3J} - a_{4kJ+j+J}) \bmod q$ 
14:       $A_{4kJ+j} \leftarrow \frac{1}{2} \cdot (T_0 + T_2) \bmod q$ 
15:       $A_{4kJ+j+J} \leftarrow \frac{1}{2} \cdot (T_1 + T_3) \cdot \omega_1 \bmod q$ 
16:       $A_{4kJ+j+2J} \leftarrow \frac{1}{2} \cdot (T_2 - T_0) \cdot \omega_2 \bmod q$ 
17:       $A_{4kJ+j+3J} \leftarrow \frac{1}{2} \cdot (T_3 - T_1) \cdot \omega_3 \bmod q$ 
18:    end for
19:  end for
20: end for
21: return  $A$ 

```

395

4 Conflict-free Memory Mapping Scheme

397 By applying loop unroll technique, a scalable iterative NTT algorithm is proposed in
 398 section 4.1. Thereafter, the general and efficient conflict-free memory mapping scheme is
 399 presented in section 4.2. Based on the scalable algorithm and memory mapping scheme,
 400 the NTT multiplication architecture can be parallelized.

4.1 Scalable Iterative NTT Algorithm

401 **Determining the order.** At the very beginning, we determine the way how the data
 402 points are managed in parallel computation. Taking DIT-NR radix-2 NTT with 2 butterfly
 403 units as an example, the 8 points data flow along with index set $\{p, k, j\}$ is depicted in Figure
 404 6. Let $G_{p,k,j}^0$ and $G_{p,k,j}^1$ denote the upper and lower point in stage p , group k and round j ,
 405 respectively. The butterfly operations with the same color belong to the same group. Then,
 406 we determine the parallel 4 data points in the second stage of 8-points INTT are fetched and
 407 stored in the following order: $\{G_{1,0,0}^0, G_{1,0,0}^1, G_{1,0,1}^0, G_{1,0,1}^1\} \rightarrow \{G_{1,1,0}^0, G_{1,1,0}^1, G_{1,1,1}^0, G_{1,1,1}^1\}$.
 408 It is easy to see that the parallel data points are managed gradually according to the
 409 growing order of index k . For 16 points radix-4 INTT with 8 parallel butterfly units, it
 410

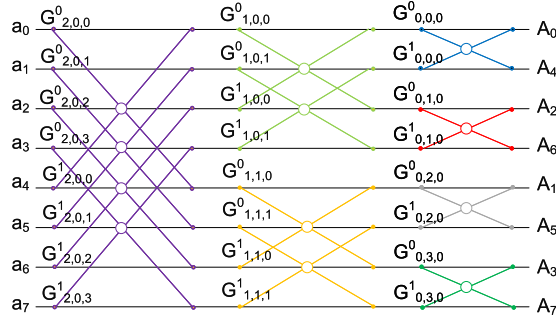


Figure 6: The data flow of 8 points radix-2 DIT-NR NTT.

411 also goes the same way with radix-2 to fetch and store the 8 data points.

412 **Scalable NTT algorithm.** We present the scalable iterative algorithm for arbitrary
 413 radix-R NTT based on the determined address order. However, applying the loop unroll
 414 method in iterative NTT algorithm directly can not lead to a perfect implementation.
 415 Because the range of index j, k in the inner loop and middle loop depends on the index p
 416 in the outer loop. The relative size of d and J will influence the number of iterations. As
 417 a result, the loop unroll method is classified into 2 cases: (1) $J < d$, the parallel data sets
 418 will contain several iterations of inner loop. (2) $J \geq d$, the inner loop will cover several
 419 parallel data sets. The scalable iterative NTT algorithm is proposed in algorithm 6. To be
 420 clear, the concrete butterfly operation is leaved out while the address generation method
 421 is kept.

4.2 Solution to Conflict Issue

423 To address the spatial conflict in section 2.2.2, we propose an efficient memory mapping
 424 scheme as belows:

N : total number of data points

r^k : radix of NTT, r is a prime, $r^k = R$

d : number of parallel butterfly units, it also stands for step size

B : number of banks, $B = R \times d$ and $N \mid B$ in the interleaved memory system

T : the total bit width of old address expressed in radix r , $T = \log_r^N$

M : the bit width of bank number value expressed in radix r , $M = \log_r^B = \log_r^{R \times d}$

C : the bit width of step size expressed in radix r , $C = T - M$

The old address a can be expressed in radix r as:

$$a = [a_{T-1}, a_{T-2}, \dots, a_1, a_0]_r = [a_{T-1}, \dots, a_{T-C}, \dots, a_{M-1}, \dots, a_1, a_0]_r$$

Expressing the lower part $[a_{M-1}, \dots, a_1, a_0]_r$ in radix B as $[b]_B$

Expressing the higher part $[a_{T-1}, \dots, a_{T-C}]_r$ in radix $R = r^k$ as $[b_{m-1}, b_{m-2}, \dots, b_0]_R$

The old address can be expressed in mixed radix $B-R$ as $a = [b_{m-1}, b_{m-2}, \dots, b_0]_R [b]_B$

Defining the step number as $SN = (b_{m-1} + b_{m-2} + \dots + b_0) \bmod R$

Then, the bank index for old address is: $BI = (b + SN \cdot d) \bmod B$

The new bank address for old address is: $BA = a \gg M = [a_{T-1}, \dots, a_{T-C}]_r$

426 The scheme is based on the mixed radix expression of the old address. It is easy to see that
 427 this memory mapping method can be implemented by a few XOR and shift operations

Algorithm 6 Scalable Iterative NTT Algorithm

Input: a denotes a vector of length N . d is the number of butterfly units. R denotes the radix of NTT.

Output: $A = Scalable_NTT(a)$

```

1: for  $p = \log_R N - 1$  to 0 do
2:    $J \leftarrow R^p$ 
3:   if  $J < d$  then
4:     for  $k = 0$  to  $N/(Rd) - 1$  do
5:       for  $i = 0$  to  $d/J - 1$  do
6:         for  $j = 0$  to  $J - 1$  do
7:           
$$\begin{bmatrix} A_0 \\ A_1 \\ \dots \\ A_{R-1} \end{bmatrix} = BF \left( \begin{bmatrix} a_{kRd+iRJ+j} \\ a_{kRd+iRJ+j+J} \\ \dots \\ a_{kRd+iRJ+j+(R-1)J} \end{bmatrix} \right)$$

8:         end for
9:       end for
10:      end for
11:    else
12:      for  $k = 0$  to  $N/(RJ) - 1$  do
13:        for  $i = 0$  to  $J/d - 1$  do
14:          for  $j = 0$  to  $d - 1$  do
15:            
$$\begin{bmatrix} A_0 \\ A_1 \\ \dots \\ A_{R-1} \end{bmatrix} = BF \left( \begin{bmatrix} a_{kRJ+id+j} \\ a_{kRJ+id+j+J} \\ \dots \\ a_{kRJ+id+j+(R-1)J} \end{bmatrix} \right)$$

16:          end for
17:        end for
18:      end for
19:    end if
20:  end for
21: return  $A$ 

```

428 if the radix is power-of-2, which is much cheaper than other methods used in [XHY⁺20]
429 [RMD⁺15]. In addition, it can support arbitrary radix NTT algorithm, conduced to
430 non-radix-2 NTT hardware design. Taking 16 points radix-2 NTT with 2 parallel butterfly
431 units as an example, the detailed mapping process is described in Figure 7. At stage 0
432 ($p = 2$), the 4 parallel data points in group 0 round 0 ($G_{2,0,0}$) and group 1 round 0 ($G_{2,1,0}$)
433 are mapped onto 4 different banks $\{0, 1, 2, 3\}$ and $\{2, 3, 0, 1\}$, respectively. By following
434 the memory mapping scheme ahead, readers should convince themselves that it also holds
435 valid for other computation stages and radice. The detailed mapping process for 27 points
radix-3 in-place NTT is also depicted in Figure 14 of appendix.

old address	mix radix R-B	step number	slide distance	bank index	bank address
0	000	(0+0)	(0x2)	(0+0) mod 4 = 0	
1	001			(0+1) mod 4 = 1	
2	002	mod 2 = 0	mod 4 = 0	(0+2) mod 4 = 2	$G_{2,0,0}$
3	003			(0+3) mod 4 = 3	
4	010			(2+0) mod 4 = 2	
5	011	(0+1)	(1x2)	(2+1) mod 4 = 3	$G_{3,0,0}$
6	012	mod 2 = 1	mod 4 = 2	(2+2) mod 4 = 0	
7	013			(2+3) mod 4 = 1	
8	100			(2+0) mod 4 = 2	
9	101	(1+0)	(1x2)	(2+1) mod 4 = 3	
10	102	mod 2 = 1	mod 4 = 2	(2+2) mod 4 = 0	$G_{2,1,0}$
11	103			(2+3) mod 4 = 1	
12	110			(0+0) mod 4 = 0	
13	111	(1+0)	(0x2)	(0+1) mod 4 = 1	
14	112	mod 2 = 0	mod 4 = 0	(0+2) mod 4 = 2	
15	113			(0+3) mod 4 = 3	11

Figure 7: The detailed memory mapping scheme for 16 points radix-2 NTT with $d = 2$.

5 Scalable Radix-2/4 NTT Multiplication Architecture

5.1 The Overall Scalable Architecture

In this section, we propose the scalable radix-2 and radix-4 NTT multiplication architecture which supports configuration for vector size N , modulus q and number of parallel butterfly units d . As shown in Figure 8, the overall architecture is composed of eight different modules. The address generator is mainly implemented by the counter and shift logic gates. The memory mapping unit consists of a few XOR logic gates and 4-to-1 or 2-to-1 multiplexers in radix-2 and radix-4 NTT, respectively. The arbiter module decodes the bank indexes as corresponding selection signals to control the path of three interconnect networks. The amount of fan-ins in radix-2 NTT interconnect network is as twice larger as that of the radix-4 NTT. Because, the number of banks in radix-2 NTT will double compared to radix-4 NTT under the same configuration of butterfly numbers. This difference will influence the performance between radix-2 and radix-4 NTT. In section 6.1, we will quantify this difference in detail. Another distinguishing feature is that the one-dimension butterfly unit in radix-2 NTT is extended in two-dimension array in radix-4 NTT, which elaborates the aforementioned difference in terms of bank number. The twiddle factors of NTT are precomputed and stored in a ROM in this architecture. Since we reuse the twiddle factors in both radix-2 and radix-4 NTT to obtain the radix-2 and radix-4 INTT, the total types of twiddle factors needs to be stored is just $N - 1$ words, which is almost half amount of the state-of-the-art designs like [XHY⁺20] and [ZYC⁺20].

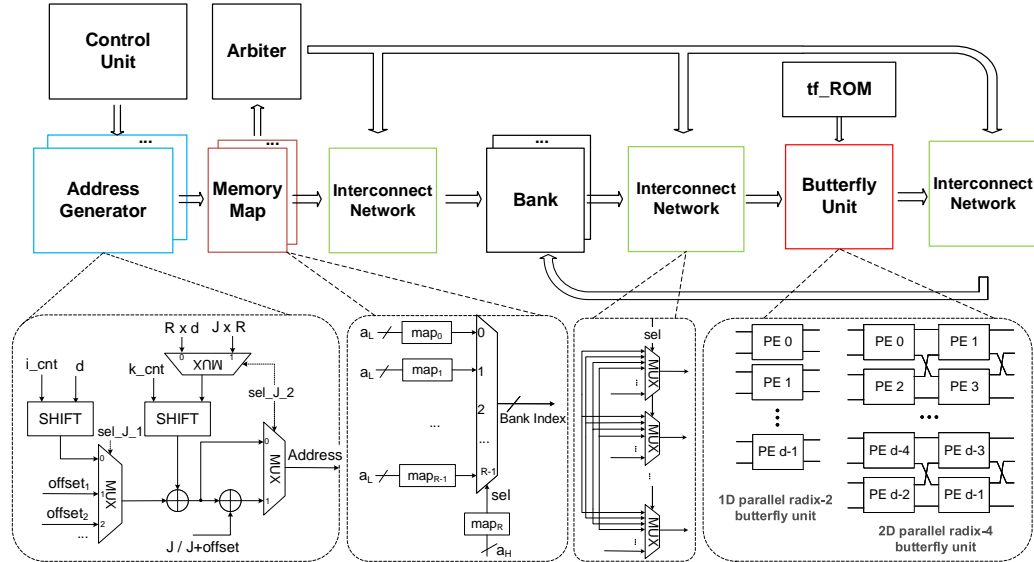


Figure 8: The scalable radix-2/4 NTT multiplication architecture.

5.2 Compact Radix-4 Butterfly Unit

As shown in section 3.3, the radix-4 butterfly unit is divided and scheduled into two-layer architecture to further reduce the computation complexity. In this section, we excavate the symmetric operator in radix-4 Cooley-Tukey and Gentleman-Sande butterfly units to reuse the hardware resource. It is observed that the IBFU1 needs an extra modular multiplication by 1/2 and the execution sequence is exactly on the contrary with BFU0.

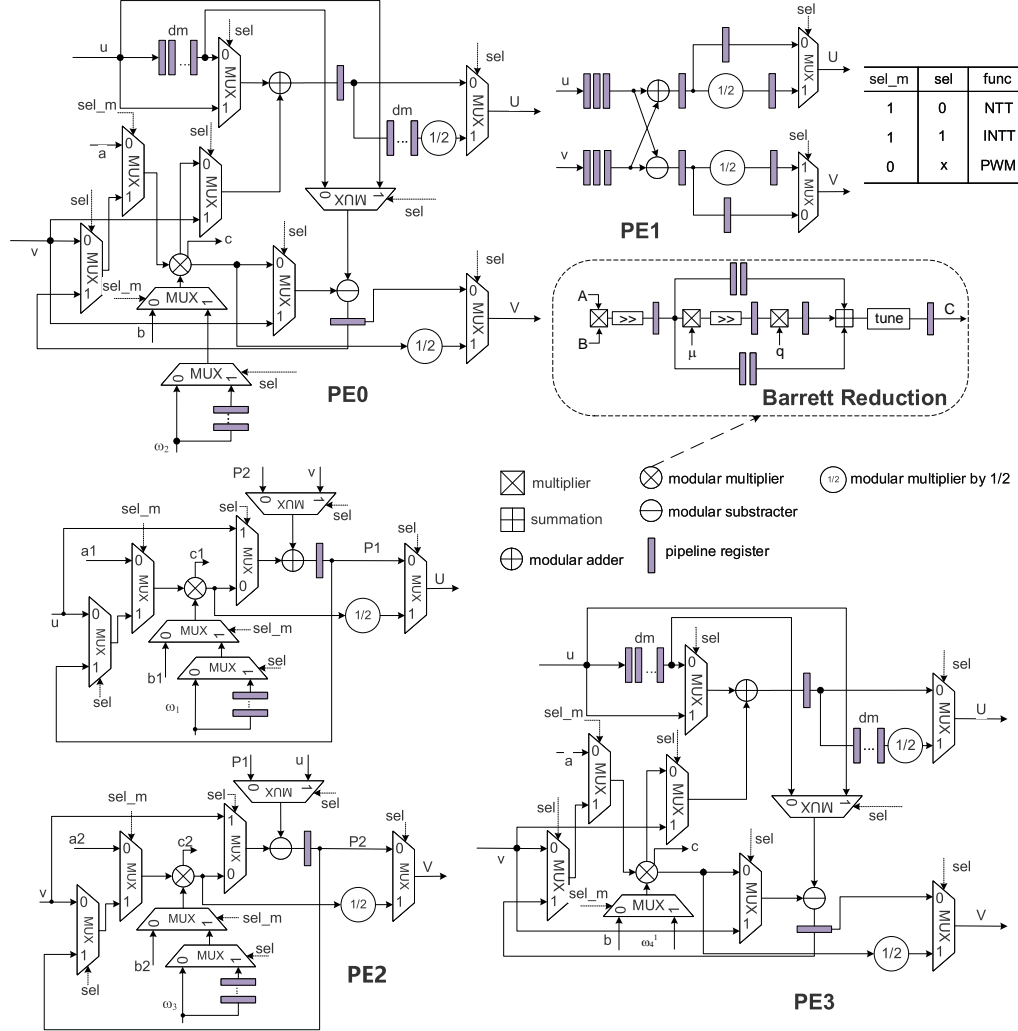
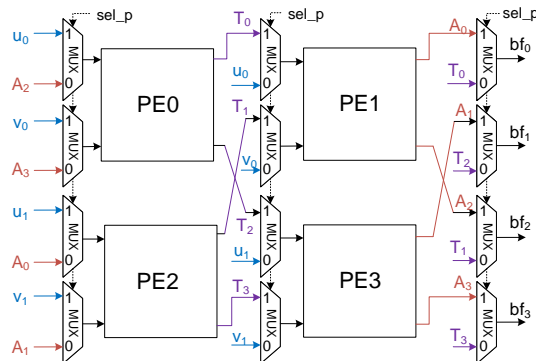


Figure 9: The compact architecture of radix-4 butterfly unit.

463 The butterfly unit pairs BFU1 and IBFU0, BFU2 and IBFU3, BFU3 and IBFU2 also
 464 have the similar difference. As a result, the DIT radix-4 NTT and DIF radix-4 INTT
 465 can be performed with 4 configurable processing elements. The Figure 9 depicts the
 466 specific architecture. When the selection signal sel_m is set to 1 and sel is set to 0 or 1,
 467 the four processing elements are configured to perform DIT NTT or DIF INTT
 468 operation, respectively. Furthermore, we also take the point wise multiplication (PWM)
 469 into consideration, which is performed by setting the signal sel_m to 1.
 470

471 So far, we just need 4 modular adders, 4 modular subtracters and 4 modular mul-
 472 tipliers to implement the NTT/INTT butterfly operation and point wise multiplication.
 473 For parametric hardware design, Montgomery reduction and Barrett reduction are two
 474 commonly used methods. [BGV93] indicates that when the bit width of modulus is less
 475 than 32 bits, using Barrett reduction is more suitable. Thus, our modular multiplier follows
 476 Barrett reduction method as shown in Figure 9. The modular multiplier is designed with
 477 four pipeline stages and the critical path is the n -bit multiplication. The parameter μ is
 precomputed for configuration.

478 The Figure 10 shows the configurable routing structure in the processing element
 479 array. When the signal sel_p is set to 1, the PEs in the first column will receive the data
 480 points fetched from the banks and finish the fist-layer butterfly operation. The PEs in
 481 the second column will receive the computation result from the first-layer and perform
 482 the second-layer butterfly operation. When the signal sel_p is set to 0, the configuration
 483 is exactly the opposite. By applying this unified PE array, the hardware resource can
 484 be reduced by approximately 50% compared to the naive implementation. It is worth to
 485 mention that unifying the radix-8 or higher-radix NTT and INTT butterfly operation will
 486 be more difficult because the symmetric property of these operators is hard to excavate
 and the routing path will become more complicated.



487 **Figure 10:** The routing structure of radix-4 PE array.

488 6 Implementation Results and Comparisons

489 The proposed architecture is designed with Verilog HDL and implemented on the 28
 490 nm Xilinx Virtex-7 FPGA (xc7vx690tffg1761-3). The resource overheads and highest
 491 frequency are obtained from Vivado 2020.2 under the default strategy for synthesis and
 492 implementation. In section 6.1, we will make a performance evaluation between radix-4 and
 493 radix-2 NTT multiplication architecture through theoretical analysis and implementation
 494 results. In section 6.2, we will compare our implementation results with the state-of-the-art
 495 works.

496 6.1 Performance Evaluation Between Radix-4 and Radix-2 NTT

497 To justify the advantages of radix-4 NTT, we compare its area-time performance with
 498 radix-2 NTT through theoretical analysis and implementation results. Table 3 shows the
 499 theoretical difference between radix-2 and radix-4 NTT in terms of hardware resources
 500 about some common modules. It is observed that the radix-4 NTT consumes the same
 501 number of cycles with radix-2 NTT, but it only needs half number of banks when configured
 502 with the same number of butterfly units. The reason for this difference is that the radix-
 503 4 NTT can perform two consecutive layers of butterfly operations, which halves the
 504 concurrent data points to be fetched at every stage. This good balance between intra-stage
 505 and inner-stage parallelization can heavily reduce the number of fan-ins of interconnect
 506 network. As shown in Table 3, the number of fan-ins in interconnect network of radix-4
 507 NTT is reduced by 91.6% compared to radix-2 NTT. In addition, the number of fan-ins in
 508 memory mapping units and address generator units of radix-4 NTT are both reduced by
 509 75% and 50%, respectively.

Table 1: The theretical comparison between radix-2 and radix-4 NTT/INTT.

Type	AGU	MMU	AB	IN	Bank	BFU	TF ROM	NTT/INTT cycle
radix-2	2d	2d× 2-to-1 MUXs	2d× 2d-to-1 MUXs	6d× 2d-to-1 MUXs	2d	d× MA/MS/MM	N - 1	(N/2d) $\log_2 N$
radix-4	d (↓ 50%)	d× 4-to-1 MUXs (↓ 75%)	d× d-to-1 MUXs (↓ 91.6%)	3d× d-to-1 MUXs (↓ 50%)	d (↓ 50%)	d× MA/MS/MM*	N - 1	(N/d) $\log_4 N$

* : Multiplying ω_4^1 (ω_4^{-1}) can be alternatively replaced with modular additions.

d : number of parallel butterfly unit

AGU : address generator unit

MMU : memory mapping unit

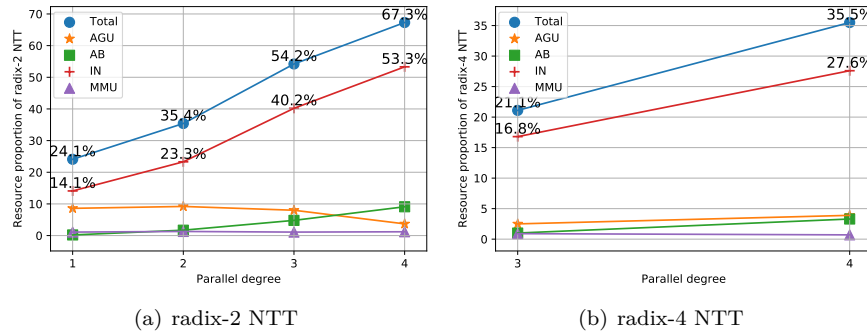
IN : interconnect network **AB** : Arbiter

BFU : butterfly unit

TF ROM : twiddle factor ROM **MA** : modular adder

MS : modular substracter

MM : modular multiplier

**Figure 11:** The variation of resource proportion with parallel degree (N = 1024, 14-bit q)

The Figure 11 indicates the variation of resource proportion with the parallel degree on the FPGA platform. The parallel degree ranges from 1 to 4, which corresponds to the number of parallel butterfly units 1, 2, 4 and 8. From this figure, we can obtain two important facts. First, it is obvious that the resource proportion of the MMU, AB and IN modules will become larger when increasing the number of parallel butterfly units in both radix-2 and radix-4 NTT. Moreover, the resource proportion of interconnect network accounts for the main part among these four modules. Second, the growth rate of resource proportion is slower in radix-4 NTT than that of radix-2 NTT. In other words, the growth rate of the number of fan-ins in radix-4 NTT is almost twice lower than that of radix-4 NTT, which promotes the area-time efficiency in radix-4 NTT. The Figure 12 with dual coordinates depicts the comparisons of ATP index in terms of different FPGA resources. The left coordinate shows that the ATP of radix-4 NTT outperforms radix-2 NTT when configured with the same number of butterfly units. This advantage is enlarged with the growth of parallel degree. When setting the number of butterfly units to 8, the improvement of ATP index achieves almost 51.6%. Moreover, the radix-4 NTT configured with 4 butterfly units achieves the best balance between area and time. The right coordinate indicates how the number of DSP and BRAM varies with the parallel degree. Since the radix-2 and radix-4 butterfly units consume the same number of modular multiplication, the growth of DSP is identical as well. But the radix-4 NTT consumes less number of BRAMs.

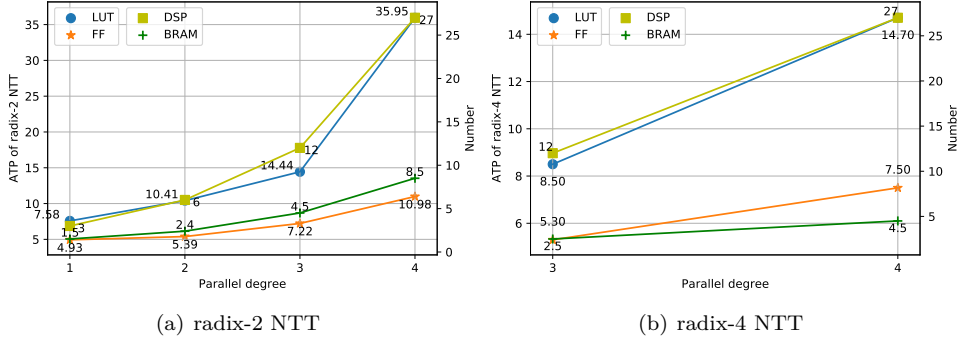


Figure 12: The variation of ATP with parallel degree ($N = 1024$, 14-bit q)

530 6.2 Comparisons with Related Work

531 Table 2 lists the key comparison results between related conflict-free memory mapping
 532 schemes and our proposed one. It is observed that the memory mapping scheme in this
 533 work can support the configuration for number of parallel butterfly units and arbitrary
 534 radix in-place NTT, which is more universe than the state-of-the-art scheme. This scheme
 535 can be implemented by simple XOR and shift logic gates as well. [XMX17] proposes a
 536 memory mapping scheme for constant geometry radix- 2^k FFT supporting any number of
 537 butterfly units, which requires double memory overheads. [FLX20] also presents a general
 538 memory mapping scheme, but it will vary with the computation stage and entangle the
 539 pipelined design. Other schemes in Table 2 neither can backup the general FFT design
 nor consumes more hardware resources and memory footprint.

Table 2: Conflict-free memory mapping scheme comparisons with related work.

Scheme	Radix Config.	BFU Config.	FFT Type	Storage	Architecture	Hardware Resource
[Joh92]	✓	✗	IP	N	Memory-based	XOR+Shift
[XMX17]	✓	✓	CG	$2N$		XOR+Shift
[RV08]	✓	✓	IP	$N \log_R N$		LUT+Shift
[BUC19]	✗	✗	CG	$2N$		XOR+Shift
[FLX20]	✗	✓	SH	$2N$		Reorder+Shift
[RVM ⁺ 14]	✗	✓	IP	N		-
[WXXY17]	✓	✓	IP	$2N$		XOR+Shift
This Work	✓	✓	IP	N	Memory-MDC-based	XOR+Shift

IP : in-place FFT. CG : constant geometry FFT. SH : Stockham FFT.

540 As shown in section 6.1, the radix-4 NTT with two-layer butterfly units owns the best
 541 ATP performance. We mainly compare its implementation results with the state-of-the-art
 542 works as depicted in Table 3. [ZYC⁺20] proposes a radix-2 NTT design with two parallel
 543 butterfly units. It cannot avoid the bit-reversed operation and consumes more than $2\times$
 544 cycles as our design. The ATP of LUT is competitive with this work. Since it proposes a
 545 fixed architecture for a specific modulus 12289, the ATP of FF and DSP is smaller than
 546 ours. However, owing to reusing the twiddle factors in NTT and INTT, our architecture
 547 achieves almost $3.9\times$ improvement in terms of BRAM ATP. [FS19] presents a radix-2 NTT
 548 design with a single butterfly unit. It consumes less BRAMs but the ATP of LUT, FF
 549 and DSP is approximately $4.8\times$, $3.1\times$ and $13.9\times$ as our work, respectively. [BUC19] puts
 550 forward a constant geometry radix-2 NTT with two parallel butterfly units as well. This
 551

design targets at power-efficiency and supports multiple modulus. Therefore, it requires less FFs but the ATP of LUT, DSP and BRAM is almost $22.8\times$, $3.6\times$ and $20.2\times$ as our design, respectively. A fast and configurable radix-2 NTT is proposed in [JGCS19]. However, it needs extra cycles to execute the bit-reversed operation, pre-processing and post-processing. The ATP of LUT and DSP is near to our work but the ATP of FF and BRAM is almost $2.3\times$ and $59.4\times$ as our design, respectively. [XL20] presents a constant geometry radix-2 NTT architecture based on 4 parallel butterfly units. However, it consumes more memory overheads and computational cycles. The ATP of LUT, FF is approximately $3.1\times$, $3.0\times$ as our design. Because the modular multiplier is specific for the modulus 12289, thus it consumes less DSPs as our design. [KLC⁺17] also puts forward a parallel radix-2 NTT architecture with 4 butterfly units. However, it cannot avoid the pre-processing and post-processing and thus needs extra more cycles. Its modular multiplier is based on a fixed Barrett reduction method for 12289. The ATP of LUT, FF, DSP and BRAM is almost $5.8\times$, $4.5\times$, $1.8\times$ and $10.7\times$ as our work, respectively. [MKO⁺20a] proposes the highly parallel radix-2 NTT with 32 butterfly units, which results in less computational cycles. Nonetheless, the high fan-out and fan-in in this architecture may pull down the maximum frequency and it does not reuse the twiddle factors. Therefore, the ATP of LUT, DSP and BRAM is nearly $3.2\times$, $1.97\times$ and $4.7\times$ as our architecture. A two-layer radix-2 in-place NTT design based on high-level synthesis method is also presented in [NDG19]. But the tricks of reusing twiddle factor and radix-4 butterfly operator are not applied in this design. It also consumes more cycles to compute NTT. As a result, the ATP of LUT, FF and BRAM is approximately $1.1\times$, $2.3\times$ and $6.6\times$ as our work.

Table 3: NTT comparisons with related work.

Work	BFU	Cycles	Freq. (MHz)	Time. (μ s)	LUT/ ATP	FF/ ATP	DSP/ ATP	BRAM/ ATP
parameters: $N = 1024$, fixed modulus $q = 12289$								
[ZYC ⁺ 20] ^A	2	2569*	244	10.5	847/8.9	375/3.9	2/21.1	6/63.2
[FS19] ^A	1	10240	-	-	980/41.1	395/16.6	26/1091	2/83.9
[BUC19] ^A	2	6155	-	-	7690/194	16/0.4	11/277.5	13/327.9
[JGCS19] ^A	1	6206*	251	24.7	343/8.5	493/12.2	3/74.2	6/148.4
[XL20] ^Z	4	2688	153	5.52	4823/26.6	2901/16.0	8/44.2	-
[KLC ⁺ 17] ^Z	4	2616*	150	17.44	2832/49.4	1381/24.1	8/139.5	10/174.4
parameters: $N = 1024$, tunable 14-bit modulus q								
[MKO ⁺ 20a] ^Z	32	200*	125	1.6	17188/27.5	-	96/153.6	48/76.8
[NDG19] ^Z	2×2	2032	188	10.81	898/9.7	1117/12.1	4/43.24	10/108.1
This work ^V	2×2	1295	200	6.5	1308/8.5	824/5.3	12/78	2.5/16.25
	4×2	655	135	4.7	3139/14.7	1595/7.5	27/126.9	4.5/21.15
	1	5125	242	21	461/9.6	235/4.9	3/63	1.5/31.5
	2	2565	232	11	946/10.4	490/5.4	6/66	2.5/27.5
	4	1285	192	6.7	2155/14.4	1078/7.2	12/80.4	4.5/30.15
	8	645	117	5.5	6537/35.9	1997/11	27/148.5	8.5/46.75

* : The cycles for bit-reversed operation are not included.

A : Artix-7 FPGA platform. V : Virtex-7 FPGA platform. Z : Zynq-7000 FPGA platform.

7 Conclusion

574 In this paper, we propose a scalable radix-2 and radix-4 NTT multiplication architecture
 576 based on an efficient memory mapping scheme. The detailed derivation process for bit-
 577 reversed-free radix-4 NTT and INTT with low complexity is provided. Both algorithm-level
 578 and architecture-level optimization techniques are applied to reduce the area overheads and
 579 memory footprint in our design. Through theoretical analysis and implementation results,
 580 we point out that the proposed radix-4 NTT-based architecture with the same number
 581 of parallel butterfly units outperforms the radix-2 one in terms of area-time performance.
 582 This advantage is enlarged when increasing the parallel degree. In addition, the proposed
 583 memory mapping scheme can support the parallelization of arbitrary radix NTT, which is
 584 more universe and efficient than other methods. In the future, we will integrate the NTT
 585 core into the PQC or FHE cryptosystem to improve the overall performance. We will also
 586 consider the protective implementations for NTT core against the side channel attacks.

587 Appendix

588 By following the deduction process in section 3 and section 4, we can still obtain the
 589 radix-3 DIT-NR in-place NTT algorithm. The concrete dataflow of 27-points radix-3
 590 DIT-NR NTT with three butterfly units is depicted in Figure 13. At every stage, 9 data
 591 points are accessed in parallel according to the growing group order. The lines with red,
 592 yellow and blue color represent the parallel butterfly operations in the first round of each
 593 stage, respectively.

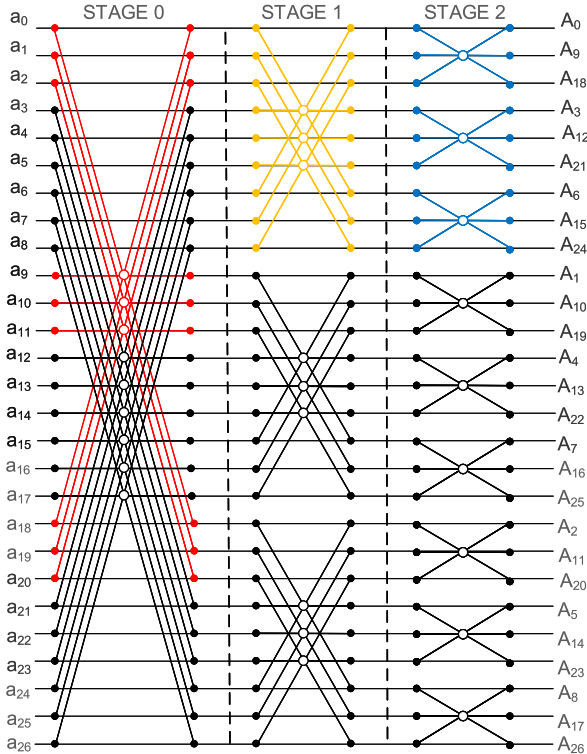


Figure 13: The dataflow of 27-points radix-3 DIT-NR NTT with $d = 3$.

594 The conflict-free memory mapping scheme proposed in section 4 is also valid for radix-3
 595 in-place NTT. The detailed mapping process for 27 points radix-3 in-place DIT-NR NTT
 596 is also depicted in Figure 14. Taking stage 0 ($p = 2$) as an example, the nine old addresses
 597 $\{0, 9, 18, 1, 10, 19, 2, 11, 20\}$ in group 0 round 0 ($G_{2,0,0}$) are mapped onto nine desired
 598 different bank indexes $\{0, 1, 2, 3, 4, 5, 6, 7, 8\}$, respectively. By derivation, readers can find
 that other computation stages also go the same way as stage 0.

old address	mix radix R-B	step number	slide distance	bank index	bank address
0	00	0 mod 3 = 0	(0x3) mod 9 = 0	(0+0) mod 9 = 0	0
1	01			(0+1) mod 9 = 1	
2	02			(0+2) mod 9 = 2	
3	03			(0+3) mod 9 = 3	
4	04			(0+4) mod 9 = 4	
5	05			(0+5) mod 9 = 5	
6	06			(0+6) mod 9 = 6	
7	07			(0+7) mod 9 = 7	
8	08			(0+8) mod 9 = 8	
9	10	1 mod 3 = 1	(1x3) mod 9 = 3	(3+0) mod 9 = 3	G _{2,0,0}
10	11			(3+1) mod 9 = 4	
11	12			(3+2) mod 9 = 5	
12	13			(3+3) mod 9 = 6	
13	14			(3+4) mod 9 = 7	
14	15			(3+5) mod 9 = 8	
15	16			(3+6) mod 9 = 0	
16	17			(3+7) mod 9 = 1	
17	18			(3+8) mod 9 = 2	
18	20	2 mod 3 = 2	(2x3) mod 9 = 6	(6+0) mod 9 = 6	2
19	21			(6+1) mod 9 = 7	
20	22			(6+2) mod 9 = 8	
21	23			(6+3) mod 9 = 0	
22	24			(6+4) mod 9 = 1	
23	25			(6+5) mod 9 = 2	
24	26			(6+6) mod 9 = 3	
25	27			(6+7) mod 9 = 4	
26	28			(6+8) mod 9 = 5	

Figure 14: The detailed memory mapping scheme for 27 points radix-3 NTT with $d = 3$.

600 References

- 601 [ABCG20] Erdem Alkim, Yusuf Alper Bilgin, Murat Cenk, and François Gérard. Cortex-
602 m4 optimizations for $\{\mathbf{R}, \mathbf{M}\}$ lwe schemes. *IACR Cryptol. ePrint Arch.*,
603 2020:12, 2020.
- 604 [ACC⁺21] Erdem Alkim, Dean Yun-Li Cheng, Chi-Ming Marvin Chung, Hülya Evkan,
605 Leo Wei-Lun Huang, Vincent Hwang, Ching-Lin Trista Li, Ruben Niederha-
606 gen, Cheng-Jhih Shih, Julian Wälde, and Bo-Yin Yang. Polynomial multipli-
607 cation in NTRU prime comparison of optimization strategies on cortex-m4.
608 *IACR Trans. Cryptogr. Hardw. Embed. Syst.*, 2021(1):217–238, 2021.
- 609 [BGV93] Antoon Bosselaers, René Govaerts, and Joos Vandewalle. Comparison of
610 three modular reduction functions. In Douglas R. Stinson, editor, *Advances in
611 Cryptology - CRYPTO '93, 13th Annual International Cryptology Conference,
612 Santa Barbara, California, USA, August 22-26, 1993, Proceedings*, volume 773 of *Lecture Notes in Computer Science*, pages 175–186. Springer, 1993.
- 613 [BKS19] Leon Botros, Matthias J. Kannwischer, and Peter Schwabe. Memory-efficient
614 high-speed implementation of kyber on cortex-m4. In Johannes Buchmann,
615 Abderrahmane Nitaj, and Tajje-eddine Rachidi, editors, *Progress in Cryptol-
616 ogy - AFRICACRYPT 2019 - 11th International Conference on Cryptology
617 in Africa, Rabat, Morocco, July 9-11, 2019, Proceedings*, volume 11627 of *Lecture
618 Notes in Computer Science*, pages 209–228. Springer, 2019.
- 619 [BUC19] Utsav Banerjee, Tenzin S. Ukyab, and Anantha P. Chandrakasan. Sapphire:
620 A configurable crypto-processor for post-quantum lattice-based protocols.
621 *IACR Trans. Cryptogr. Hardw. Embed. Syst.*, 2019(4):17–61, 2019.
- 622 [CG99] E. Chu and A. George. *Inside the FFT Black Box*. Inside the FFT Black
623 Box, 1999.
- 624 [CHK⁺21] Chi-Ming Marvin Chung, Vincent Hwang, Matthias J. Kannwischer, Gregor
625 Seiler, Cheng-Jhih Shih, and Bo-Yin Yang. NTT multiplication for ntt-
626 unfriendly rings new speed records for saber and NTRU on cortex-m4 and
627 AVX2. *IACR Trans. Cryptogr. Hardw. Embed. Syst.*, 2021(2):159–188, 2021.
- 628 [CMV⁺15] Donald Donglong Chen, Nele Mentens, Frederik Vercauteren, Sujoy Sinha Roy,
629 Ray C. C. Cheung, Derek Chi-Wai Pao, and Ingrid Verbauwhede. High-speed
630 polynomial multiplication architecture for ring-lwe and SHE cryptosystems.
631 *IEEE Trans. Circuits Syst. I Regul. Pap.*, 62-I(1):157–166, 2015.
- 632 [FL19] Xiang Feng and Shuguo Li. Accelerating an FHE integer multiplier using
633 negative wrapped convolution and ping-pong FFT. *IEEE Trans. Circuits
634 Syst. II Express Briefs*, 66-II(1):121–125, 2019.
- 635 [FLX20] Xiang Feng, Shuguo Li, and Sufen Xu. Rlwe-oriented high-speed polynomial
636 multiplier utilizing multi-lane stockham NTT algorithm. *IEEE Trans. Circuits
637 Syst. II Express Briefs*, 67-II(3):556–559, 2020.
- 638 [FS19] T. Fritzmann and J. Sepulveda. Efficient and flexible low-power ntt for lattice-
639 based cryptography. In *2019 IEEE International Symposium on Hardware
640 Oriented Security and Trust (HOST)*, 2019.
- 641 [Gen09] C. Gentry. Fully homomorphic encryption using ideal lattices. *Stoc*, 2009.

- 643 [GGMG13] Mario Garrido, Jesús Grajal, Miguel A. Sánchez Marcos, and Oscar Gustafsson. Pipelined radix- 2^k feedforward FFT architectures. *IEEE Trans. Very Large Scale Integr. Syst.*, 21(1):23–32, 2013.
- 644
- 645
- 646 [GOPS13] Tim Güneysu, Tobias Oder, Thomas Pöppelmann, and Peter Schwabe. Software speed records for lattice-based signatures. In Philippe Gaborit, editor, *Post-Quantum Cryptography - 5th International Workshop, PQCrypto 2013, Limoges, France, June 4-7, 2013. Proceedings*, volume 7932 of *Lecture Notes in Computer Science*, pages 67–82. Springer, 2013.
- 647
- 648
- 649
- 650
- 651 [GS66] W. M. Gentleman and G. Sande. Fast fourier transforms: for fun and profit. *ACM*, 1966.
- 652
- 653 [HT96] Shousheng He and Mats Torkelson. A new approach to pipeline FFT processor. In *Proceedings of IPPS '96, The 10th International Parallel Processing Symposium, April 15-19, 1996, Honolulu, Hawaii, USA*, pages 766–770. IEEE Computer Society, 1996.
- 654
- 655
- 656
- 657 [JGCS19] Arpan Jati, Naina Gupta, Anupam Chattopadhyay, and Somitra Kumar Sanadhya. Spqcop: Side-channel protected post-quantum cryptoprocessor. *IACR Cryptol. ePrint Arch.*, 2019:765, 2019.
- 658
- 659
- 660 [Joh92] L. G. Johnson. Conflict free memory addressing for dedicated fft hardware. *IEEE Trans. on Circuit and Systems-II*, 39(5):312–316, 1992.
- 661
- 662 [KLC⁺17] Po-Chun Kuo, Wen-Ding Li, Yu-Wei Chen, Yuan-Che Hsu, Bo-Yuan Peng, Chen-Mou Cheng, and Bo-Yin Yang. High performance post-quantum key exchange on fpgas. *IACR Cryptology ePrint Archive*, page 690, 2017.
- 663
- 664
- 665 [LNS20] Vadim Lyubashevsky, Ngoc Khanh Nguyen, and Gregor Seiler. Practical lattice-based zero-knowledge proofs for integer relations. In Jay Ligatti, Xinxing Ou, Jonathan Katz, and Giovanni Vigna, editors, *CCS '20: 2020 ACM SIGSAC Conference on Computer and Communications Security, Virtual Event, USA, November 9-13, 2020*, pages 1051–1070. ACM, 2020.
- 666
- 667
- 668
- 669
- 670 [LSW01] Hsin-Fu Lo, Ming-Der Shieh, and Chien-Ming Wu. Design of an efficient FFT processor for DAB system. In *Proceedings of the 2001 International Symposium on Circuits and Systems, ISCAS 2001, Sydney, Australia, May 6-9, 2001*, pages 654–657. IEEE, 2001.
- 671
- 672
- 673
- 674 [MAA⁺20] Dustin Moody, Gorjan Alagic, Daniel Apon, David Cooper, Quynh Dang, John Kelsey, Yi-Kai Liu, Carl Miller, Rene Peralta, Ray Perlner, Angela Robinson, Daniel Smith-Tone, and Jacob Alperin-Sheriff. Status report on the second round of the nist post-quantum cryptography standardization process, 2020-07-22 2020.
- 675
- 676
- 677
- 678
- 679 [MKO⁺20a] Ahmet Can Mert, Emre Karabulut, Erdinc Ozturk, Erkay Savas, and Aydin Aysu. An extensive study of flexible design methods for the number theoretic transform. *IEEE Transactions on Computers*, pages 1–1, 2020.
- 680
- 681
- 682 [MKÖ⁺20b] Ahmet Can Mert, Emre Karabulut, Erdinç Öztürk, Erkay Savas, Michela Becchi, and Aydin Aysu. A flexible and scalable NTT hardware : Applications from homomorphically encrypted deep learning to post-quantum cryptography. In *2020 Design, Automation & Test in Europe Conference & Exhibition, DATE 2020, Grenoble, France, March 9-13, 2020*, pages 346–351. IEEE, 2020.
- 683
- 684
- 685
- 686
- 687

- 688 [NDG19] Duc Tri Nguyen, Viet B. Dang, and Kris Gaj. A high-level synthesis approach
689 to the software/hardware codesign of ntt-based post-quantum cryptography
690 algorithms. In *International Conference on Field-Programmable Technology, FPT 2019, Tianjin, China, December 9-13, 2019*, pages 371–374. IEEE, 2019.
- 692 [Nic71] Peter J. Nicholson. Algebraic theory of finite fourier transforms. *Journal of Computer and System Sciences*, 5(5):524–547, 1971.
- 694 [POG15] Thomas Pöppelmann, Tobias Oder, and Tim Güneysu. High-performance
695 ideal lattice-based cryptography on 8-bit atxmega microcontrollers. In Kristin E. Lauter and Francisco Rodríguez-Henríquez, editors, *Progress in Cryptology - LATINCRYPT 2015 - 4th International Conference on Cryptology and Information Security in Latin America, Guadalajara, Mexico, August 23-26, 2015, Proceedings*, volume 9230 of *Lecture Notes in Computer Science*,
696 pages 346–365. Springer, 2015.
- 698 [RMD⁺15] Stephen Richardson, Dejan Markovic, Andrew Danowitz, John Brunhaver,
700 and Mark Horowitz. Building conflict-free FFT schedules. *IEEE Trans. Circuits Syst. I Regul. Pap.*, 62-I(4):1146–1155, 2015.
- 702 [RV08] Dionysios I. Reisis and Nikolaos Vlassopoulos. Conflict-free parallel memory
704 accessing techniques for FFT architectures. *IEEE Trans. Circuits Syst. I Regul. Pap.*, 55-I(11):3438–3447, 2008.
- 706 [RVM⁺14] Sujoy Sinha Roy, Frederik Vercauteren, Nele Mentens, Donald Donglong
708 Chen, and Ingrid Verbauwhede. Compact ring-lwe cryptoprocessor. In Lejla Batina and Matthew Robshaw, editors, *Cryptographic Hardware and
710 Embedded Systems - CHES 2014 - 16th International Workshop, Busan, South Korea, September 23-26, 2014. Proceedings*, volume 8731 of *Lecture Notes in Computer Science*, pages 371–391. Springer, 2014.
- 712 [Sho94] P.W. Shor. Algorithms for quantum computation: discrete logarithms and factoring.
714 In *Proceedings 35th Annual Symposium on Foundations of Computer Science*, pages 124–134, 1994.
- 716 [Sto06] H. S. Stone. R66-50 an algorithm for the machine calculation of complex
718 fourier series. *IEEE Transactions on Electronic Computers*, EC-15(4):680–681, 2006.
- 720 [SYJ84] E.E. Swartzlander, W.K.W. Young, and S.J. Joseph. A radix 4 delay commutator for fast fourier transform processor implementation. *IEEE Journal of Solid-State Circuits*, 19(5):702–709, 1984.
- 722 [TCH19] Wei-Lun Tsai, Sau-Gee Chen, and Shen-Jui Huang. Reconfigurable radix-
724 $2^k \times 3$ feedforward FFT architectures. In *IEEE International Symposium on Circuits and Systems, ISCAS 2019, Sapporo, Japan, May 26-29, 2019*, pages 1–5. IEEE, 2019.
- 726 [TJS03] J.H. Takala, T.S. Jarvinen, and H.T. Sorokin. Conflict-free parallel memory
728 access scheme for fft processors. In *Proceedings of the 2003 International Symposium on Circuits and Systems, 2003. ISCAS '03.*, volume 4, pages IV–IV, 2003.
- 730 [WHEW14] Wei Wang, Xinming Huang, Niall Emmart, and Charles C. Weems. VLSI
732 design of a large-number multiplier for fully homomorphic encryption. *IEEE Trans. Very Large Scale Integr. Syst.*, 22(9):1879–1887, 2014.

- 733 [XHY⁺20] Guozhu Xin, Jun Han, Tianyu Yin, Yuchao Zhou, Jianwei Yang, Xu Cheng,
734 and Xiaoyang Zeng. Vpqc: A domain-specific vector processor for post-
735 quantum cryptography based on risc-v architecture. *IEEE Transactions on*
736 *Circuits and Systems I: Regular Papers*, 67(8):2672–2684, 2020.
- 737 [XL20] Yufei Xing and Shuguo Li. An efficient implementation of the newhope key
738 exchange on fpgas. *IEEE Trans. Circuits Syst. I Regul. Pap.*, 67-I(3):866–878,
739 2020.
- 740 [XL21] Yufei Xing and Shuguo Li. A compact hardware implementation of cca-secure
741 key exchange mechanism CRYSTALS-KYBER on FPGA. *IACR Trans.*
742 *Cryptogr. Hardw. Embed. Syst.*, 2021(2):328–356, 2021.
- 743 [XMX17] Qianjian Xing, Zhen-guo Ma, and Yingke Xu. A novel conflict-free parallel
744 memory access scheme for FFT processors. *IEEE Trans. Circuits Syst. II*
745 *Express Briefs*, 64-II(11):1347–1351, 2017.
- 746 [WXXY17] Kaifeng Xia, Bin Wu, Tao Xiong, and Tian-Chun Ye. A memory-based FFT
747 processor design with generalized efficient conflict-free address schemes. *IEEE*
748 *Trans. Very Large Scale Integr. Syst.*, 25(6):1919–1929, 2017.
- 749 [ZYC⁺20] Neng Zhang, Bohan Yang, Chen Chen, Shouyi Yin, Shaojun Wei, and
750 Leibo Liu. Highly efficient architecture of newhope-nist on FPGA using
751 low-complexity NTT/INTT. *IACR Trans. Cryptogr. Hardw. Embed. Syst.*,
752 2020(2):49–72, 2020.